Photodiagnosis and Photodynamic Therapy 27 (2019) 255–267

Contents lists available at ScienceDirect

Photodiagnosis and Photodynamic Therapy

journal homepage: www.elsevier.com/locate/pdpdt

Photodynamic therapy for the treatment of oral squamous carcinoma—Clinical implications resulting from *in vitro* research

Marcin Olek[a], Jacek Kasperski[a], Dariusz Skaba[b], Rafał Wiench[b], Grzegorz Cieślar[c], Aleksandra Kawczyk-Krupka[c,*]

[a] School of Medicine with the Division of Dentistry in Zabrze, Medical University of Silesia in Katowice, Department of Prosthetic Dentistry, Chair of Prosthetics and Dental Materials, Akademicki Sq. 17, 41-902 Bytom, Poland
[b] School of Medicine with the Division of Dentistry in Zabrze, Medical University of Silesia in Katowice, Department of Periodontal Diseases and Oral Mucosa Diseases, Traugutta Sq. 2, 41-800 Zabrze, Poland
[c] School of Medicine with the Division of Dentistry in Zabrze, Medical University of Silesia in Katowice, Department of Internal Medicine, Angiology and Physical Medicine, Center for Laser Diagnostics and Therapy, Batorego Street 15, 41-902 Bytom, Poland

ARTICLE INFO

Keywords:
Oral cavity squamous cell carcinoma
Photodynamic therapy
Cell culture
Photosensitizer
Two-dimensional model
Three-dimensional spheroids
The chicken chorioallantoic membrane

ABSTRACT

Background: Oral cavity squamous cell carcinoma is a common cancer of the head and neck region. Due to the frequency of diagnoses, high rate of mortality, mutilating nature of classic therapy and numerous complications, new methods of treatment are being sought. One promising solution for treatment which is utilized in many fields of oncology is photodynamic therapy. The purpose of this article is to present a general overview of the use of photodynamic therapy in preclinical in vitro studies.
Materials and methods: A literature search for articles corresponding to the topic of this review was performed using the PubMed and MEDLINE databases using the following keywords: 'oral cavity squamous cell carcinoma,' 'photodynamic therapy,' 'photosensitizer(s),' 'in vitro,' 'cell culture(s),' 'spheroids,' 'CAM model', and 'in vivo.'
Results: Most of the previous work found in the literature search concerns research on the use of various photosensitizers and the determination of their level of phototoxicity against cell lines.
Concluding remarks: Research on the photodynamic effect in cell lines may be useful in establishing the mechanisms and effectiveness of the photodynamic method as a starting point for clinical trials. Studies on spheroidal models allows for testing photodynamic therapy under more clinical-like conditions. The Chick Chorioallantoic Membrane Assay provides information about the vascular changes after treatment.

1. Introduction

Apart from nonmelanoma skin cancer, oral cavity squamous cell carcinoma (OSCC) is the most frequent malignant tumor of the head and neck. It accounts for 90% of histopathological diagnoses of malignant lesions in the oral cavity. In 2012, around 300,000 new patients were diagnosed with the disease [1,2]. This type of cancer develops more often in men and the risk of positive diagnosis increases with age [3]. The most common risk factors are stimulants such as tobacco smoking, consumption of alcohol, or betel chewing. In the case of combined abuse, the risk is multiplied [1,4–7]. The most prevalent location of OSCC is the tongue, especially its lateral border, and the floor of the mouth. Other areas of the oral cavity are less affected by this malignancy (Fig. 1) [1,8].

The role of tobacco smoking, alcohol use, poor oral hygiene, periodontal diseases, candidiasis, nitrosamines, radiation, and human papillomavirus (HPV) infections in connection of OSCC is well-documented. Oral carcinogenesis is a progressive disease from normal epithelium through dysplasia to invasive phenotypes. The genetic aberrations observed in the pathological lesions are the mutations in p53, c-erbB2, or in the epidermal growth factor receptor (EGFR). Abnormal expressions of EGFR, K-ras, H-ras, Pl3K, c-myc, int-2, PTEN, transforming growth factor-alpha (TGF-α), and B-cell lymphoma (BCL) like oncogenes have been implicated in OSCC development (Fig. 2).

The basic method of therapy includes surgical resection leaving a margin of healthy tissue. It is accompanied by neck dissection when node metastases are detected. In some cases, postoperative adjuvant radiotherapy is applied [8,9]. Classic therapy often leads to impaired oral functions, for instance, speech problems, dysphagia, difficulties with mastication, or mobility disorders of the head and neck region

* Corresponding author.
E-mail address: akawczyk@gmail.com (A. Kawczyk-Krupka).

https://doi.org/10.1016/j.pdpdt.2019.06.012
Received 23 March 2019; Received in revised form 16 June 2019; Accepted 17 June 2019
Available online 18 June 2019

Fig. 1. Oral cancer.

[10–12]. In turn, radiotherapy leads to complications such as xerostomia, radiation caries, taste disorders, mucositis, or even osteoradionecrosis [13–15]. Development of alternative methods of treatment is being pursued due to the mutilating character of the therapy and its potential complications.

One promising method of treatment is photodynamic therapy (PDT) [16,17]. PDT utilizes photosensitizers (PSs) administered systemically or locally with the subsequent use of light at the appropriate intensity and wavelength. As a result, reactive oxygen species (ROS) are formed leading to the destruction of the tumor by either cell necrosis or apoptosis [18–20]. The use of such a method for OSCC treatment is dependent on the cancer stage. The thickness of the diseased tissue is particularly important, as it is directly related to the light penetration depth. The best candidates for this therapy are patients with a cancer infiltration of less than 5 mm with no lymph node metastases [21]. The advantages of PDT are the possible use of local anesthesia and a small postoperative scar if any [13,21].

This literature review presents the results of preclinical in vitro studies on OSCC cell lines (Table 1), spheroids, and Chick Chorioallantoic Membrane (CAM model). The PubMed and MEDLINE databases were explored using the following keywords: 'oral cavity squamous cell carcinoma,' 'photodynamic therapy,' 'photosensitizer(s),' 'in vitro,' 'cell culture(s),' 'spheroids,' 'CAM model,' and 'in vivo.'

2. Photodynamic effect on OSCC cell lines – two-dimensional models

2.1. Porphyrin-mediated photodynamic effect on OSCC cells

Choi et al. investigated the effect of hematoporphyrin phototoxicity on the KB cell line. Irradiation with light at 635 nm and 5 mW/cm^2 was performed after 3 -hs of incubation. The study showed a 50% reduction in cell survival. Necrosis and apoptosis were measured by flow cytometry, DNA fragmentation, and Diff-Quick staining. Using a confocal microscope, the distribution of the PS was ascertained successively in the cell membrane, cytoplasm, and cell nucleus [22].

In turn, Lai et al. examined the phototoxic effect of hematoporphyrin monomethyl ether (HMME) on tongue squamous cell carcinoma cells (Tca8113). After irradiation with light at 530 ± 20 nm with fluence between 0.6–3.0 J/cm^2, significant cell proliferation inhibition, as well as apoptosis and necrosis were observed with a predominance of apoptosis. Phototoxicity enhancement correlated with an increase in the level of PS and radiant exposure. Using a confocal microscope, the largest accumulation of HMME was found in the mitochondria. PDT also increased the activity of caspase-3 in the Tca8113 cells [23].

Singlet oxygen, formed during the collision of photo-excited PS with oxygen, reacts with polyunsaturated fats of the cell membrane, causing the formation of lipid peroxides. Ferrous ions (Fe^{2+}) are needed to form free radicals from lipid hydroperoxides and ascorbic acid is a reducing agent that can reduce iron from the ferric to the ferrous oxidation state. Accordingly, Kelley et al. investigated the impact of iron and ascorbic acid on the phototoxicity of sodium porfimer on SCC-25 cells. The researchers observed a time-dependent increase in the production of free radicals. The cells were incubated in 15 μg/mL sodium porfimer. Then, 20 μM $FeSO_4$ and 100 μM ascorbic acid were added to the test sample. The cells were then exposed to visible light. There was a decline in cell survival in the presence of these pro-oxidants [24].

2.2. ALA-mediated photodynamic effect on OSCC cells

Fang et al. studied the effect of an expression of microRNA-145 on cells that underwent PDT with 5-Aminolevulinic acid (5-ALA). In their research, they used SAS and GNM lines which were incubated for three hours with PS and then exposed to red light at 635 ± 5 nm wavelength. The researchers found an overexpression of mRNA-145 in the irradiated cells, which correlated with the inhibition of cell growth, increased level of apoptosis, and reduced invasiveness and underexpression of CD44 [25].

A dissimilar level of susceptibility to PDT may lead to selective cell death. Sharma et al. compared the phototoxic effect of 5-ALA on macrophages isolated from mouse peritoneal and two OSCC cell lines: NT8e and 4451. The tests were performed for various serum concentrations (0–10%) in cell culture. The cells were incubated for 15 h with 200 μg/ml 5-ALA. Then, the protoporphyrin IX (PpIX) level was assessed by spectrofluorometry. A far greater level of PpIX was found in the macrophages, whereas the amount of PS increased with the decrease of serum concentration in all cultures of both cancer cells and macrophages. Phototoxicity after irradiation with light at 630 ± 20 nm and 70 mW/m^2 were similar. For the serum concentration of 10%, no phototoxic activity was found for cancer cells using the MTT assay; the phototoxicity for the macrophages reached 20% compared to the control group (no 5-ALA and no light). Without serum, the phototoxicity for the macrophages reached 78% and for the 4451 line, it was 19%. There were no significant differences in the viability of the two cancer cell lines. In the case of PDT on the common cultures of macrophages (human or mouse) and cancer cells, selective death of the macrophages was reported [26].

Researchers are also constructing light sources to reduce the costs of therapy using commercially available devices. Tsai et al. examined the phototoxic effect of 5-ALA-induced Pp-IX on gingival squamous cell carcinoma cell line (Ca9-22). After a 3 -h incubation in 5-ALA at 100 mM, cells were exposed to light from two different sources. The first was a lab-constructed LED source with a wavelength maximum at 635 ± 5 nm and a fluence of 100 mW/cm^2. The second light source was a commercial VersaLight® device in a wavelength range of around 580–720 nm and a 100 mW/cm^2 fluence rate. No statistically significant differences were found in cell viability by MTT assay. For the commercial device, the LD50 was 4.5 J/cm^2, while for the handmade device, it was 4.3 J/cm^2 [27].

Cells originating from different topographic spaces may have different susceptibility levels to therapy. Yang, T. H. et al. analyzed the phototoxic effect of 5-ALA on Ca9-22 and KJ-1 (nasopharyngeal carcinoma line). After a 3 -h incubation at 1 mM of 5-ALA, the cells were exposed to red light (633 nm) with a doses from 0 to 6 J/cm^2. The positive doses caused a decrease in cell viability by MTT assay. The OSCC cells were more sensitive to PDT (LD_{50}~0.5 J/cm^2) than the KJ-1 cells (LD_{50}~3 J/cm^2). After the cells were exposed to sub-lethal doses of PDT, decreased migration and invasiveness of both cell lines were found by wound healing assay, migration assay, and Matrigel invasion assay. In turn, in Western Blot study, a decrease in the phosphorylation of extracellular signal-regulated kinase (ERK), Src kinase, and focal adhesion kinase (FAK) was noticed, which had an impact on the aforementioned decrease in both migration and invasion [28].

One way of improving the effectiveness of PDT is to combine therapy with other agents. Yang, D.F. et al. examined the effect of calcipotriol (CAL) on the phototoxicity of 5-ALA. SCC4 and SAS cell lines were used in this study. Initially, the cells were treated with CAL for 72 h at concentrations of 0-10^{-5} M. Then, they were incubated for four hours in 5-ALA (0-0.375 mM). After that, cells were exposed to 640 nm light with 10 J/cm^2 fluence. Compared to the control group,

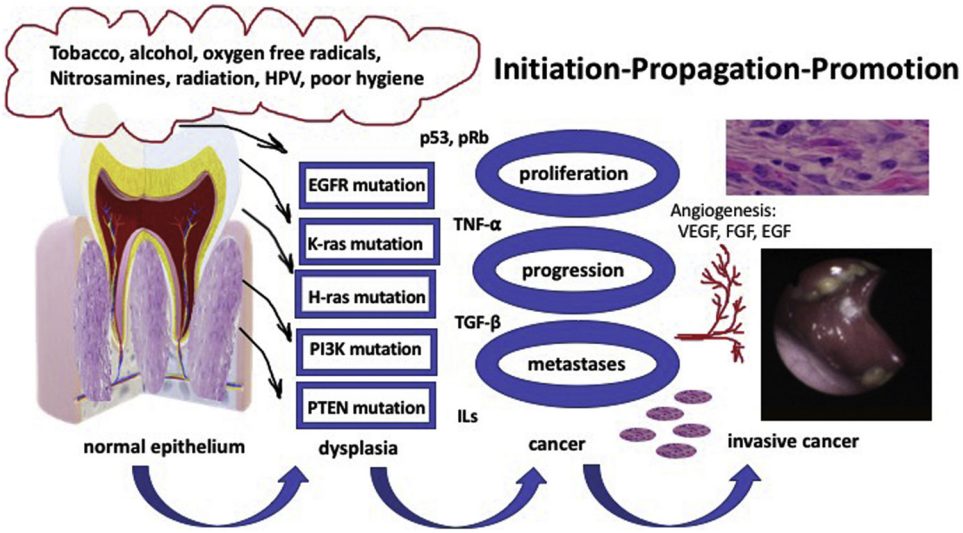

Fig. 2. Simplified schema of oral cancer development. Vascular endothelial growth factor (VEGF), epidermal growth factor (EGF), epidermal growth factor receptor (EGFR), tumor necrosis factor α (TNF-α), transforming growth factor β (TGF- β), phosphatase and tensin homolog (PTEN), fibroblast growth factor (FGF), interleukins(ILs), p53 cellular tumor antigen, tumor suppressor, Rb protein (pRb, tumor suppressor), PI3K, K-ras, H-ras: proteins.

there was a significant reduction in the survival of cells that had been previously treated with CAL. Based on the results of the study, it was concluded that 10^{-8} M CAL concentration was the most suitable for inhibiting cell survival for 0.125, 0.25 or 0.375 mM of 5-ALA. Western Blot showed an increased expression of the CPOX enzyme, which is involved in PpIX synthesis in the CAL-treated cells [29].

Another study by Yang, D.F. et al. was conducted to determine the effectiveness of methotrexate (MTX) and ALA-PDT combined therapy against the SCC4 cell line. In the beginning, the cells were pre-incubated for 72 h at various concentrations of MTX (0–1 mg/L). The next step was 4 -hs of incubation at 0-0.375 mM ALA. Finally, the cells were irradiated with light with same wavelength and fluence used in the previous study. The authors reported a significant increase in cell mortality in the MTX-ALA-PTD treated group compared to the control group by MTT assay. An increased CPOX activity in the cells was demonstrated by Western Blot, specifically for MTX concentration of 0.001 mg/L [30].

A possible way to increase the effectiveness of therapy is through PS intracellular metabolism. Yamamoto et al. investigated the effect of Ferrochelatase (FECH) and the ATP-binding cassette G2 transporter inhibitors (ABCG2; factors affecting the accumulation of PpIX in cells) on the level of effectiveness of PDT. HSC-4 cell lines were incubated for three hours in 0–2 mM 5-ALA, with or without fetal bovine serum, and with various combinations of the inhibitors. They were then irradiated with light at λ = 600–700 nm and with fluence equal to 9.6 J/cm^2. The presence of plasma significantly reduced the PpIX accumulation in cancer cells. The use of the FECH and ABCG2 inhibitors and their combinations resulted in an increased PS accumulation in the cells and increased PDT efficacy of cell mortality growth. The cell death pathway was apoptosis dependent on caspase [31].

Chen, H. M. et al. determined the exact death pathway Ca9-22 cells in their study. The cells were incubated for three hours at 1 mM of 5-ALA. They were divided into five groups which had been exposed to mitogen-activated protein kinases (MAPK) and NF-κB inhibitors before irradiation. Subsequently, the cells were exposed to light at 635 ± 5 nm and with fluence equal to 4 J/cm^2. It was found by Western Blot analysis that PDT caused a significant increase in caspase-8 and caspase-9 activity. In turn, when inhibitors were used, apoptosis was suppressed. This indicated the existence of two pathways in OSCC leading to apoptosis, which was associated with the death receptor and mitochondrial-dependent. In the case of treating cells with JNK and NF-κB inhibitors, apoptosis was almost completely inhibited. Based on these results, it was concluded that apoptosis occurred on the NF-κB-JNK signaling pathway in the Ca9-22 cells [32].

An important aspect of the accumulation of PS in the cell is its ability to undergo transmembrane transport. Moon, Y. H. et al. tested the use of self-synthesized ALA-hexenyl ester (ALA-hx) and compared it with ALA. Tongue squamous cell carcinoma line (YD10B) was incubated in the 5 μM solution of each PS for four hours. Next, the cells were irradiated with light at 613–645 nm wavelengths and 5 J/cm^2 fluence. The researchers showed ALA-hx to have a greater effect on cell viability causing it to fall by 85% within 24 h after PDT. For comparison, the same concentration of ALA had no such significant effect on cell survival. In the case of ALA-hx and with the use of a fluorescent microscope, higher levels of PpIX were observed in the cells. The researchers suggested that the higher efficacy with ALA-hx may be due to esterification and thus enhanced lipophilic character. By showing the increased number of the cells stained by Annexin V in flow cytometry as well as the increased activity of caspase-3, it can be concluded that the main way of cell death was apoptosis [33].

Under PDT's influence, various cell lines may show different pathways of cell death. In addition to apoptosis and necrosis, another mechanism that can induce programmed cell death is autophagy. Wang et al. verified the photodynamic effect of methyl aminolevulinate (MAL) on dysplastic oral keratinocyte line (DOK) and Ca9-22. The cell cultures were incubated at 7.5 mM of MAL for 16 h and then irradiated with red light with 6 J/cm^2 fluence and 200 mW/cm^2 fluence rate. The researchers found reduced viability of the DOK line. They also noted cell death occurred by the autophagic pathway, which could be observed using a transmission electron microscope. There was an increase in the expression of p62/SQSTM1 and LC3II, which indicated autophagy. For Ca9-22, there was also a decrease in viability, however, no autophagic cell death was observed. The increased expression of proapoptotic proteins, terminal deoxynucleotidyl transferase dUTP nick end labelling (TUNEL), and flow cytometry analysis results indicated apoptosis of these cells [34].

One of the important features of cancer cells that can be used in combination therapy is cyclooxygenase (COX)-2 expression. In the first stage of the research, Akita et al. determined the level of COX-2 expression in biopsy materials taken from healthy tissues as well as from precancerous and cancerous changes of the skin and oral mucosa. A raised level of COX-2 expression was noticed with increasing levels of dysplasia. The next stage was a study on two cell lines: HSC-2 with a high expression of COX-2 and HSC-4 with a complete lack of COX-2 expression. The cells were irradiated with light at 630 nm and with 20–120 J/cm^2 fluence after having been incubated in 5-ALA (1 mmol/L). Nimesulide was used as the COX-2 inhibitor. Dose-dependent inhibition was demonstrated only for HSC-2. The synergistic effect of nimesulide and ALA-PDT on the HSC-2 cells was found using MTT analysis. For the HSC-4 cells, there was no statistically significant

Table 1
PDT of OSCC —preclinical studies in vitro.

Cell line(s)	Photosensitizer(s)	Radiation	Reference
KB	hematoporphyrin	635 nm and 5 mW/cm^2	Choi et al.[22]
Tca8113	Hematoporphyrin monomethyl ether 1.25, 2.5, and 5 μg/ml	530 ± 20 nm, 0.6–3.0 J/cm^2	Lai et al.[23]
SCC-25	porfimer sodium 15 μg/ml	Visible light	Kelley et al.[24]
SAS and GNM	5-Aminolevulinic acid	635 ± 5 nm at various doses	Fang et al.[25]
NT8e and 4451	5-Aminolevulinic acid 200 mg/ml	630 ± 20 nm, 7 mW/m^2, 8.4 kJ/m^2	Sharma et al.[26]
Ca9-22	5-aminolevulinic acid 1 mM	580–720 nm, 100 mW/cm^2, 0–8 J/cm^2	Tsai et al.[27]
Ca9-22, KJ-1	5-aminolevulinic acid 1 mM	633 nm	Yang, T. H. et al.[28]
SCC4, SAS	5-aminolevulinic acid 0–0.375 mM	640 nm, 10 J/cm^2	Yang, D.F. et al.[29]
SCC4	5-aminolevulinic acid 0–0.375 mM	640 nm, 10 J/cm^2	Yang, D.F. et al.[30]
HSC-4	5-aminolevulinic acid 0–2 mM	600–700 nm, 9.6 J/cm^2	Yamamoto et al.[31]
Ca9-22	5-aminolevulinic acid 1 mM	635 ± 5 nm, 4 J/cm^2	Chen, H. M. et al.[32]
YD10B	hexenyl ester of ALA 5 mM	613–645 nm (peak 635 nm), 5 J/cm^2, 35 mW/cm^2	Moon, Y. H. et al.[33]
DOK, Ca9-22	methyl aminolevulinate 7.5 mM	Red light, 6 J/cm^2, 200 mW/cm^2	Wang et al. [34]
HSC-2, HSC-4	5-aminolevulinic acid 1 mM/L	630 nm, 70 mW/cm^2, 20–120 J/cm^2	Akita et al.[35]
HSC-3 cell	NPe6 1.0 mg/ml	664 nm, 0.1–100 J/cm^2, 150 mW/cm^2	Nakagawa et al.[36]
CAL-27	chlorin(e6) and hyperbranched poly(ether-ester) 1–150 μM	660 nm, 12 J/cm^2, 100 mW/cm^2	Li et al.[39]
HSC-3 and SCC-25	Chlorin e6 50 μM/100 μM + nimotuzumab/cetuximab 50 μg/ml/100 μg/ml	665 nm, 1 J/cm^2	Bhuvaneswari et al.[38]
H376, VB6, UP	m-THPC 0.25–4 mg/ml	652 nm, 0.25 and 4 J/cm^2, 25 mW/cm^2	Sharwani et al.[37]
SAS and HSC-4	PAD-S31 1–00 μg/ml	670 nm, 1–30 J/cm^2	Date et al.[40]
YD-10B	Pheophorbide a 0–2 μM	664 nm, 4.24 J/cm^2	Ahn et al.[41]
FaDu and FaDu-PTX	Pheophorbide a 0.2–0.5 μM	613–64 nm, 1.2 or 2 J/cm^2	Kim et al.[42]
YD10B, YD38, IHOK	Pheophorbide a 0.3 μM	664 nm, 0.5 J/cm^2	Moon, S. et al.[43]
oral (HSC2 and HSC3) and nasopharyngeal (HK1 and C666-1)	151-hydroxypurpurin-7-lactone ethyl methyl diester 0.1-3 mM, pheophorbide-a 0.1-3 mM	> 600 nm, 2.9–14.4 J/cm^2	Lim, S. H. et al.[44]
KB, U87MG, SKOV3, FaDu, LNCap, A549	Pheophorbide-a conjugates 0-2 μM	613–645 nm, 1.25 J/cm^2, 35 mW/cm^2	You et al.[45]
Cal27	Rose Bengal 10 μM	530 ± 15 nm, 1.6 J/cm^2, 20 mW/cm^2	Song et al.[46]
KB	Indocyanine green 0.2–250 μM	640 nm, 785 nm, 895 nm	Lim, H. J. et al.[47]
H357 and DOK	Erythrosine b 71.03–1136.5 μM	500–550 nm, 81.72 J/cm^2 and/or 122.58 J/cm^2	Garg et al.[48]
KB	chloroaluminum-phthalocyanine 5 mM	670 nm, 25 J/cm^2, 40 mW/cm^2	Tapajos et al.[49]
HSC-2, HCT-116, MCF-7	zinc (II) phthalocyanines 0.01–100 μM	> 580 nm, 4.0 J/cm^2, 7.5 mW/cm^2	Chin et al.[50]
HN ACC 417	curcumin 0.1–1 μg/ml	1 J/cm^2 UVA or visible light	Beyer et al.[51]
KB	aloe emodin,40 μmol/L	405 nm, 40 mW/cm^2	Liu et al.[52]
OECM-1	methylene blue (nanocomposite) 250 μg/mL	980 nm, 1,5 W/cm^2	Chen et al. [53]
CAL-27	Titanium dioxide (nanocomposite) 1 mM	980 nm, 675 J/cm^2, 2.1 W/cm^2	Lucky et al.[54]
HSC-3, H413	Diazepinoporphyrazines(liposome nanodelivery) 0.05–10 μM	690 nm, 3.6 J/cm^2, 3.0 mW/cm^2	Piskorz et al.[55]
HSC-3, HR13	magnesium(II) and zinc(II) phthalocyanines	Various light properties	Wierzchowski et al.[56]
FaDu	Al(III) phthalocyanine chloride disulfonic acid 1 μg/ml	λ = 670 nm, 0.15–0.75 J/cm^2, 0.5 to 2.5 mW/cm^2	Trinidad et al.[57]
OSC-19, HeLa, SW620	IRDye700DX 0–100 nM	670 ± 10 nm, 4 mW/cm^2	van Driel et al.[58]

difference between ALA-PDT alone and ALA-PDT with nimesulide. Double immunostaining with Annexin V demonstrated apoptosis and cell death [35].

2.3. Chlorin-mediated photodynamic effect on OSCC cells

Exhaustive testing of PDT can led to elucidation of mechanisms at the cellular level. An important aspect for carcinogenesis is the levels of vascular endothelial growth factor (VEGF) and proto-oncogenes expression. Nakagawa et al. investigated the effect of PDT, using mono-l-aspartyl chlorin e6 (NPe6), on the level of VEGF: c-jun and c-fos expressions in HSC-3 cells. After the treatment, the cells with PS at a concentration of 1 μg/mL were irradiated with light at 664 nm wavelength and with 10 J/cm^2 fluence. A utilizing enzyme linked immunosorbent assay (ELISA) and reverse transcription polymerase chain reaction (RT-PCR), causing an increase in the level of VEGF. The highest level of the same expression was found after eight hours of irradiation. Then, the level decreased. The next stage of the study was to show an increase in the level of VEGF and its dependence on dose. The cells were incubated in PS in 0–10 μg/mL concentration range and then treated with 0.1–100 J/cm^2 light. The VEGF level was evaluated eight hours after PDT. Once the cells were exposed to PDT, the expression level of the proto-oncogenes, c-jun and c-fos, was also evaluated. The researchers noted an increase. The expression of mRNA responsible for the synthesis of all the aforementioned proteins was inhibited by SB203580 and p38 MAPK. Cycloheximide inhibited the mRNA expression for VEGF, whereas N-acetyl-L-cysteine reduced and increased the expression for c-jun and c-fos respectively [36].

Sharwani et al. used sublethal doses of *m*-tetra(hydroxyphenyl) chlorin (m-THPC) and light to investigate the influence of PDT on the

expression of matrix metalloproteinases (MMPs), VEGF, and urokinase plasminogen activators (uPA) in H376, VB6, and UP cell lines. Initially, the sublethal doses were determined by phototoxicity curve analysis. To establish the level of activity of these proteins, ELISA and zymography were used. After PDT, a reduced amount of both active and inactive forms of MMP-2 and MMP-9 was found in both UP and VB6 lines, whereas in H376 line, the active form of MMP-2 was upregulated. As for MMP-13, PDT caused a 19-45-fold decrease in expression of H376, but for VB6, it led to a 1.6-fold increase compared to control groups. In VB6 and HPC6 cell lines, the VEGF expression was reduced in measurement 24 and 48 h after PDT. No significant differences were noted for UP. Additionally, to examine the activity of uPA, a chromogenic assay was conducted. A significant reduction in expression was noted only for VB6 [37].

There is a high expression of EGFR in OSCC. One of the goals of therapy is its inhibition. Researchers are looking for combination therapies that would work synergistically. Bhuvaneswari et al. examined the use of PDT and EGFR inhibitors in their work. After overnight incubation with various combinations of PSs (chlorin e6 and the anti-EGFR monoclonal antibodies nimotuzumab and cetuximab), HSC-3 and SCC-25 cell lines were treated with light at 665 nm wavelength and with 1 J/cm^2 fluence. They demonstrated the synergistic activity of PDT and EGFR inhibitors. In combination therapy, a significant increase in the antitumor activity was noticed [38].

To increase the uptake of PSs and photodynamic activity, various researchers focus on the molecular structure of the PS. Li et al. verified the phototoxicity of combined hyperbranched polymers: hyperbranched poly(ether-ester) and PS-chlorin(e6) (HPPE-ce6). The photodynamic effect of HPPE-ce6 was examined as well as its location in CAL-27 line of tongue cancer. Light at 660 nm wavelength and 12 J/cm^2 fluence was used to activate the PS. The conjugate showed greater phototoxicity than free ce6 (3–4 times lower cell survival) by MTT assay. The main place of accumulation of HPPE-ce6 was cytoplasm, as verified by confocal microscopy. The authors suggested that an increase in the effectiveness of the therapy may have been due to an increase in PS uptake by cells, more appropriate distribution in the cells, or a lower susceptibility to self-aggregation [39].

Date et al. exposed SAS and HSC-4 lines to diode laser light at λ = 670 nm and 1–30 J/cm^2 fluence. The cells were incubated prior in 1–100 μg/ml of PAD-S31 (a hydrophilic chlorin) for two hours. A WST-8 assay was performed to determine cell viability. A 90% reduction in cell survival was noted in the exposure conditions with 20 J/cm^2 fluence and a PAD-S31 concentration of 30 μg/mL. Using TUNEL assay and ELISA test, an increase in apoptosis after PDT was demonstrated [40].

2.4. Bacteriochlorin-mediated photodynamic effect on OSCC cells

Ahn et al. analyzed the phototoxicity of Pheophorbide a (Pa) that was synthesized from chlorophyll-a obtained from an ethnopharmacological herb. In their study, they used the YD-10B cell line. The cells were treated with Pa for two hours and then irradiated with diode laser light at 664 nm wavelength and 4.24 J/cm^2 fluence. Mitochondrial membrane potential and ROS were investigated. Using fluorescence microscopy and Annexin V staining, an increase in the number of apoptotic cells was noted. The researchers also indicated an increased level of autophagy by advancing the amount of LC3B-II and accumulation of acidic vesicular organelles. The suppression of autophagy with chloroquine caused cytotoxicity through necrosis [41].

Drug-resistant cells pose a problem to therapeutic modalities, hence the need for treatment methods that can overcome such obstacles. Kim et al. confronted the receptivity of the FaDu cell line and its derivative: the multi-drug resistant line (MDR; FaDu-PTX) which is received by incubation with paclitaxel. After 24 -h incubation in Pa, the cells were treated with light at λ = 613–645 nm and with 1.2 or 2 J/cm^2 fluence. There was high cytotoxicity in both groups of the cells with a noticeably higher level of apoptosis in the FaDu cells. The researchers marked a high expression of HOXC6 and multidrug resistance-1 gene in the MDR cell line, however, PDT reduced the expression of these genes. The authors also pointed to the synergistic activity of low interference of RNA for both HOXC6 and PDT. This may have been evidence of inhibition of tumor growth by reducing the expression of HOXC6 and MDR-1 genes by PDT [42].

Another protein affecting the susceptibility of cells to PDT is runt-related transcription factor 3 (RUNX-3). Moon, S. et al. tested the phototoxic effects of Pa on OSCC cell lines (YD10B, YD38) and two immortalized human oral keratinocytes (IHOK) cell subgroups simulating premalignant changes. The IHOK cells came from one cell line, but they differed in morphology. IHOK (S) and IHOK (P) were of spindle and polygonal shape respectively. Each line was incubated in 0.3 μM of Pa for two hours and then treated with light at 664 nm and with 0.5 J/cm^2 fluence. Using MTT assay, decreased cell viability was noted after PDT for both cancerous and precancerous cells. For YD10B and YD38 lines, a reduction of cell survival was 70% and 60% respectively. Such a difference was statistically significant. As far as the IHOK cells are concerned, their viability was reduced by 70% in IHOK (S), and by 45% in IHOK (P), which is also a statistically significant difference. For a number of apoptotic cells, the results were similar. A statistically significant higher amount of YDB10 than YD38, and IHOK (S) than IHOK (P) was noted. In addition to the phototoxicity study, the researchers focused on determining the influence of the expression level of the runt-related transcription factor 3 (RUNX-3) gene on its responsiveness to PDT. Using Western Blot Analysis, they confirmed that the higher the expression of RUNX-3 in cells, the more sensitive they are to PDT. In the case of siRNA blocking the gene, the viability of previously more susceptible cells increased [43].

Researchers are still looking for new compounds that could serve as PSs in PDT. To assess their suitability, it is necessary to compare them with an already tested compound. Lim, S. H. et al. compared Pa with a newly extracted PS from the Araceae plant 151-hydroxypurpurin-7-lactone ethyl methyl diester (compound 1). Four cell lines were used in the study: HSC2, HSC3 (OSCC cell lines), HK1, and C666-1 (nasopharyngeal cancer cell lines). During the first four hours of incubation in both types of PS, a rapid increase in Pa uptake was found. After that time, the amount of Pa in the cells remained at the same level, while for compound 1, it increased during the next 20 h. Therefore, a 4 -h incubation period was selected for further study stages. Once incubated in dilutions of PS in the range of 0.1–3.0 μM, the cells were irradiated with light at > 600 nm wavelength and with fluence equal to 2.9–14.4 J/cm^2. With the use of MTT assay, a statistically significant lower inhibitory concentration (IC50) was observed for compound 1 in the radiant exposure of 14.4 J/cm^2. Extensive apoptosis was noted for compound 1 compared to Pa [44].

To improve the selectivity of PDT, PSs are combined with moieties that bind to cancer cell receptors. By using targeted therapy, damage to the normal tissue surrounding the tumor can be avoided. You et al. studied PDT efficacy with the use of Pa conjugates with four different cancer-targeting moieties: folic acid, CRGDLASLC peptide, cRGDfK peptide, and leuprorelin. The research was conducted on six different cell lines, including the OSCC line, which differed in the expression of receptors for the given conjugates. In the study of cellular uptake that used confocal microscopy, a significantly high level of the PS-conjugates was found in the cells with the high receptor expression compared to the receptor-negative cells. The activity of PDT in vitro has also been determined in both positive- and negative-receptor pairs for the mentioned moieties. The cells were treated with the PS-conjugates for two hours and then with light at 613–645 nm wavelength and a light dose of 1.25 J/cm^2. The most selective therapy turned out to be towards the FaDu cells, which had a high number of $\alpha_v\beta_6$ receptors for the CRGDLASLC peptide. It was found that cell death occurred mainly through apoptosis. The research showed that Pa-CRGDLASLC peptide conjugate could be an effective tool in selective PDT against OSCC with

the high expression of $\alpha_v\beta_6$ [45].

2.5. Synthetic dyes-mediated photodynamic effect on OSCC cells

Song et al. tested the phototoxicity of rose Bengal (RB) on the CAL-27 cell line. The cells were incubated for one hour in 10 μM o RB and then irradiated with light at 530 ± 15 nm wavelength, with 1.6 J/cm^2 fluence and 20 mW/cm^2 fluence rate. Three times more ROS were found in the cells after PDT than in the control group. Decreased cell viability and growth were demonstrated by MTT assay. In flow cytometry measurements, an increased amount of Annexin V stained cells was found, indicating the induction of ROS dependent apoptosis. The researchers also evaluated O_2 and Ca^{2+} fluxes in non-invasive microtest technique. The O_2 and Ca^{2+} fluxes affected the regulation of apoptosis and were considered good exponents. Western Blot analysis was also performed, which showed increased expression levels of cytochrome c, cleaved caspase-3, cleaved caspase-9, and poly ADP ribose polymerase (PARP) [46].

Lim, H. J. et al. investigated the effect of PDT with indocyanine green (ICG) on KB cells. The highest absorbance for ICG was found at 788 nm wavelength. Using MTT analysis, a half maximal inhibitory concentration (IC50) was tested at different wavelengths of light. For irradiation at 785 nm, IC50 reached 10 μM, whereas, for 640 nm and 895 nm, it was 300 μM and 120 μM respectively. The researchers did not find a statistically significant difference in phototoxicity for various incubation times in ICG, which indicated quick uptake of PS by cells. Both apoptosis and necrosis were observed, with the latter more often marked at the higher levels of PS and longer incubation time. The authors suggested using ICG in larger size tumors due to the absorption peak at 788 nm wavelength (infrared range), which allows for deeper light penetration in tissue [47].

An important aspect for prognosis is early detection and lesion removal, especially before the change undergoes a neoplastic transformation. Researchers have demonstrated greater susceptibility of precancerous cells than cancerous cells at the cellular level. Garg et al. compared PDT with erythrosine b activated at 500–550 nm of light irradiation on tongue squamous cell carcinoma cells (H357) and dysplastic oral keratinocytes (DOK). The findings showed that pre-malignant cells (DOK) were more susceptible to therapy than malignant cells (H357). Exposed to the radiation reaching 122.58 J/cm^2 and concentration of erythrosine being 1136.5 μM, approximately 60% of H357 and about 80% of the DOK cells were killed. The PS accumulated mainly in the mitochondria in both types of cells. However, major changes in the mitochondrial membrane potential were found in the case of DOK. In the event of high concentrations of erythrosine, severe necrosis of DOK was observed, whereas, with H357, both apoptosis and necrosis were reported [48].

Phthalocyanines (Pcs) could also be included in the synthetic dyes group of PS. Tapajos et al. studied the photodynamic effect of chloroaluminum-Pc (AlClPc) on KB cells. The cells were incubated at 5 μM of AlClPc for 30 min. After such time, the cells were exposed to continuous-wave laser light at 670 nm wavelength, with fluence equal to 25 J/cm^2 and fluence rate of 40 mW/cm^2. The researchers found 80% cell death after two hours from PDT by a trypan blue cell viability test. The percentage continued increasing 24 h after treatment. Acridine orange/ethidium bromide (AO/EB) staining assay showed necrosis as the main pathway of cell death, which was also confirmed by the evaluation of cell morphology with light and electron microscopy. Comet analysis was also conducted, which proved 70% fragmentation of DNA in the cells subjected to PDT [49].

The pharmacokinetics of PSs is an important factor for the efficacy of PDT. Although Pcs are a great candidate for PDT, their use is limited by low solubility in water and tendency to aggregate. Chin et al. studied the impact of the insertion of glycerol molecules to Zn(II) phthalocyanine (ZnPc) on singlet oxygen generation, cellular uptake, and phototoxicity. In this study, three modifications of ZnPc (marked with numbers 1, 2, and 3) and tetrasulfonated ZnPc(ZnPcS4) as standard were used. Compound 1 was characterized by tetra-glycerol peripheral substitution, compound 2 by tetra-glycerol non-peripheral substitution and compound 3 by 3 mono-iodo peripheral and tri-glycerol-non-peripheral substitution. The authors found a 2.5× higher singlet oxygen production rate for compounds 1, 2, and 3 than for ZnPcS4. The uptake studies conducted on HSC-2 line showed 20 times greater uptake of compound 3 than ZnPcS4 in the first two hours. The change in the uptake for other modifications was not statistically significant. Phototoxicity was measured on three cell lines: MCF-7 (human breast carcinoma), HCT-116 (human colon carcinoma), and HSC-2 (OSCC). After incubation in the solutions of PSs of 0.01–100 μM concentration range, the cells were irradiated with light at 630 nm wavelength and with fluence equal to 20–120 J/cm^2. Importantly, irradiation was carried out with the PS in the medium. The strongest in vitro cytotoxic activity showed compound 3 with IC50 equal to 0.04-0.06 μM, which is 60 times more than for compound 2. For ZnPcS4 and compound 1, no statistically significant decrease in cell viability was found [50].

2.6. Natural products-mediated photodynamic effect toward OSCC cells

Beyer et al. examined the phototoxic effect of low curcumin concentration against OSCC cell line (HN ACC 417), spontaneous immortalized human keratinocyte cell line (HaCaT), and human epidermoid carcinoma cell line (A431). After one hour of incubation in solution at 0.1–1 μg/mL concentration of curcumin, cells were irradiated with 1 J/cm^2 UVA or visible light. The findings showed changes in cells morphology, raised activity of lactate dehydrogenase, impaired DNA synthesis, and DNA fragmentation, which are the exponents of apoptosis [51].

Liu et al. reported the use of aloe emodin (AE) in PDT. After a 4 -h treatment of the KB cell line with 40 μmol/L aloe emodin solution, cells were irradiated with light at 405 nm wavelength. With the use of wound healing assay, a reduced ability of the KB cancer cell migration was demonstrated. Using a fluorescence microscope and flow cytometry, a significant increase of ROS was observed in the cells compared to the control group. In Western Blot, there was also an increased level of caspase-3 and Bax. In turn, a decreased amount of Bcl-2 may have indicated cell death by apoptosis [52].

2.7. Nanoparticles and nano-mediated photodynamic effect on OSCC lines

A relatively new method to increase the effectiveness of PDT is the utilization of PS composed of nanomaterials. This enables, among other things, to increase the concentration of the PS in the irradiated area and, consequently, increase the level of ROS. In one study, Chen C.W. et al. used methylene blue (MB) encapsulated in a silica shell (SiO_2). They also created a nanocomposite containing upconversion nanoparticles (UCNs) combined with gold nanorods (AuNRs). The aim of UCNs is to convert near-infrared (NIR) (980 nm) into light at a wavelength that can excite MB. The advantage of using NIR is a deeper wave penetration, which is directly connected to the PDT effectiveness at a greater depth of tissue. In turn, AuNRs increase the efficiency of UCNs, resulting in an increased ROS production. In the conducted in vitro studies on OSCC line (OECM-1), cells were incubated for 24 h at 250 μg/mL of the created nanocomposite (UCP@SiO2-NR-FA). The cells were then exposed to light at λ = 980 nm and 1.5 W/cm^2 fluence rate. The researchers, using Alamar Blue assay, found that 70% of the cells died under these conditions. The main pathway of cell death was apoptosis, ascertained by caspase-3 activity and JC-1 staining [53].

In turn, Lucky et al. used titanium dioxide (TiO_2) as a PS. TiO_2 is stimulated in the UV light range, therefore, the use of UCNs was necessary for the use of NIR. The nanoparticle was made of a UCN core covered with a thin layer of silica to improve solubility in water. The PS was the last layer of the nanoparticle. Finally, the surfaces were modified with silane groups of maleimide-polyethylene glycerols (Mal-PEG)

to limit the formation of aggregates and greater cellular uptake. High production of ROS was noted after the exposure of both TiO_2-UCNs and Mal-PEGTiO_2-UCNs to NIR. In the study of cellular uptake that was carried out on OSCC and mouse macrophages, PEGylation was shown to significantly increase the uptake by cancer cells with the reduced macrophage uptake. CAL-27 was exposed to 980 nm light (NIR) and fluence equal to 675 J/cm^2. In light-alone conditions, the survival of over 95% of the cells was noted. For 1 mM Mal-PEG-TiO_2-UCNs and 1 mM TiO2-UCNs, the irradiation resulted in the death of 78% and 56% of the cells respectively [54].

The use of nanocarriers enables to increase the efficiency of PDT. One of the most promising methods is the use of liposomes. Liposomes allow for overcoming limitations, such as aggregation propensity, poor water solubility, low bioavailability, or limited tissue penetration. Piskorz et al. investigated the PTD efficacy of three synthesized diazepinoporphyrazines (PZs): magnesium(II) diazepinotribenzoporphyrazine (1), magnesium(II) diazepinoporphyrazine (2), and demetalated diazepinoporphyrazine (3). The researchers found that the PS used had a lower level of ROS production than ZnPc used as a control. The most effective ROS generator turned out to be PZ1, while PZ3 was the least effective. In vitro tests were performed on two OSCC lines: HSC-3 and H413. The cells were incubated for 24 h in a solution of PZ1 at concentrations equal to 0.05, 0.25, and 1 μM. They were also incubated with PZ2 and PZ3 at a concentration of 0.1, 1, and 10 μM for the same time period. Then, they were exposed to light at a wavelength of 690 nm radiant exposure with 3.6 J/cm^2 fluence and 3.0 mW/cm^2 light irradiance. By Alamar Blue assay, H413 cell viability was reduced by 90% and around 25% for PZs1 (1 μM) and PZs2 (10 μM) respectively. There was no statistically significant difference for PZs3. In turn, for HSC-3 cell line, viability was reduced by circa 95% and 87% for PZs1 (1 μM) and PZs3 (10 μM) respectively. For PZs2, no light-dependent cytotoxicity was found. The research was performed with PZ1 and PZ3 on the HSC-3 line, using encapsulated forms. In the case of the PZs1 enclosed in liposomes, the effectiveness of therapy was almost 3 times higher than of the free PS. As far as PZ3 is concerned, phototoxic effects were not demonstrated on the encapsulated forms [55].

Wierzchowski et al. evaluated the properties and suitability for PDT of four newly synthesized magnesium phthalocyanines (MgPc) and ZnPc derivatives marked with numbers from Pc-1 to Pc-4. Pc-1, Pc-3, and Pc-4 are MgPc derivatives containing the following substituents: polyether, both polyether and heterocyclic, and only heterocyclic correspondingly. Pc-2 is a ZnPc derivative with polyether substituents. The most effective molecule in the production of ROS turned out to be Pc-2. OSCC cell lines (HSC-3 and HR13) were incubated at various concentrations of a PS that did not cause dark cytotoxicity. After incubation in Pc-1, Pc-2, and Pc-3, the cells were exposed to light at λ = 600–850 nm. The Pc-4 cells were irradiated at a wavelength equal to 735 nm. The strongest phototoxic activity in vitro was the Pc-3 molecule, even though it was not the best ROS generator. The next stage of the research was to determine the effectiveness of PDT with the use of encapsulated forms in liposomes as a delivery system. The encapsulation of Pc-1 and Pc-3 failed, therefore, only Pc-4 was used for this part. The phototoxicity of the liposome-enclosed form was found to be twice as high as of free Pc-4 [56].

Another way to increase the effectiveness of treatment is combined therapy. A possible solution is to combine photothermal therapy (PTT) with PDT. Trinidad et al. tested combined PTT and PDT therapies on the FaDu line. For PTT, silica-gold nanoshells (AuNs) and macrophage delivery were used. As for PDT, the cells were incubated in Al(III) phthalocyanine chloride disulfonic acid at a concentration of 1 μg/mL for 18 h and then were exposed to light at 670 nm wavelength with 0.15–0.75 J/cm^2 fluence and at 0.5–2.5 mW/cm^2 fluence rate. The researchers showed a strong synergistic effect of both types of therapy. Single PDT and PTT therapies had a low impact on the reduction of cell survival, but combined therapy reduced viability to less than 40% in the same conditions as in single therapy. Another conclusion is the confirmation of the effectiveness of using macrophages as AuNs conveyors [57].

To limit side effects, such as damaged healthy tissues, antibody delivery is used. However, this method also has its limitations, that is, prolonged photosensitivity, reduced PS penetration and, consequently, reduced PDT efficiency. Therefore, the use of nanobodies as a targeted PDT method was developed. Van Driel et al. investigated the use of IRDye700DX as a PS conjugated to nanobodies which selectively bind to cells with a high level of EGFR expression. In this in vitro study, three cell lines with different expressions of EGFR were tested: OSSC line (OSC-19) with a high expression, cervical cancer line (HeLa) with an intermediate expression, and colorectal cancer (SW620) with a low expression. Three nanobodies, that is, 7D12 (bound to domain III of EGFR), 7D12-9G8 (bound to two different epitopes), and R2 (control nanobody that did not bind to EGFR) were used in the experiment. The cells were irradiated with light with the following properties: 670 ± 10 nm wavelength and 4 mW/cm^2 fluence rate after being incubated in the conjugated PS in the 0–1 mM concentration range. In cell binding assay, fluorescence correlated with EGFR expression. The highest phototoxicity was observed for the 7D12-9G8-PS conjugate. IC50 reached the level of 2.2 ± 0.97 nM in the OSCC line study. It was marked that the efficacy of PDT was dependent on the level of EGFR expression in cell lines [58].

3. Research on OSSC three-dimensional models

New curative methods and drugs are being tested in cell culture systems to determine their effectiveness. There are two models available: a classic two-dimensional (2D) model and three-dimensional (3D) spheroids. The former has its limitations, that is, an inability to mimic the conditions of the physiological cell-cell interactions observed in solid tumors, artificial environment parameters, and a negative impact on clinical trials. The 3D cell culture systems have a list of advantageous features. One of them is creating better tumor microenvironments that help with the formation of the extracellular matrix (ECM) and deliver more precise proliferation rates, cellular morphology, and physiology. 3D cell cultures reflect similar conditions to those in vivo tumors. Multi-cellular 3D spheroids were explored first in 1970 using glioblastoma cells [59].

Many authors emphasize the role of microenvironments in 2D and 3D models of different cancer cells. The cells in 3D spheroids are much more susceptible to different therapeutic methods, hence a greater possibility to predict the clinical response of new treatment modalities. The 3D cell culture models are commonly seen to be superior to monolayer cultures; however, there are only a few studies that support the use of spheroid models in head and neck cancers (HNSCC).

Nurmenniemi et al. used human tongue squamous cell carcinoma (HSC-3) cells and HNSCC cells in a 3D model to define and create a more authentic environment for carcinoma cells. In this experiment, the researchers assessed the quantification of invasion and proliferation with in situ hybridization, Western Blotting, and analysis of collagen metabolites by radioimmunoassays. The authors concluded that the organotypic 3D model duplicated the in vivo environment more thoroughly than 2D cell culture experiments in vitro, and provided a promising tool for the analysis of the behavior of the carcinoma cells [60].

Kadletz et al. compared the differences between the 3D spheroids and a 2D model of the following HNSCC cell lines: FaDu, CAL27, and SCC25. Differences were found in proliferation rates and biomarkers expression, highlighting a significant divergence of cell growth and release of cytokines. The authors revealed that multicellular spheroids were a reliable method to imitate the immunohistochemical characteristics of tumor cells observed in solid tumors [61].

Essid et al. examined the cell culture system of the HNSCC cell line (CAL33) using a 3D spheroid model. The study revealed that the spheroid CAL33 cells underwent an epithelial-mesenchymal transition (EMT). Hypoxia, EGF, and fibroblast growth factor (FGF) were essential

for the activation of EMT [62].

Progressing OSCC may infiltrate adjacent bones. Patient prognosis is also affected in the case of previous bone invasions. Hwang et al. determined the molecular basis of a bone invasion induction process based on clinical trials, 3D cell culture studies, and animal models. In their research, they tested the possibility of using insulin-like growth factor-II mRNA binding protein-3 (IMP3) and podoplanin (PDPN) as possible targets for anti-tumor therapy. In retrospective studies, they showed a correlation between the level of the IMP3 and PDPN expressions with the level of tumor malignancy. To confirm that outcome, the researchers performed another test on 3D cultures of YD-10B cells that showed high expression of the above two proteins. Two clones of the cells were created using shRNA lentiviral particles. The first one was deprived of IMP3 protein and the second of PDPN. There was a significant decrease in invasion index for cell clones compared to wild-type cells [63].

The conditions of hypoxia in HNSCC are associated with adverse prognosis due to an increased risk of metastasis and neoplastic infiltration. Brusevold et al. examined the development of an organotypic model of invasive OSCC, using PE/CA-PJ49 tongue cancer line treated with cobalt chloride ($CoCl_2$). 3D cell culture study was carried out on the collagen matrix together with normal fibroblasts. Immunohistochemical studies showed an increased expression of phosphorylated extracellular signal-regulated kinases 1 and 2 (p-ERK1 / 2), COX-2, p75 NTR, and hepatocyte growth factor receptor (Met), and confirmed their role as indicators of cell invasion. Moreover, these results were similar to the results obtained from OSCC biopsies. In the created model, there was an increase in the fragmentation of type IV collagen constituting the cell membrane component and the islands of cancer cells formed in the matrix compared to the control group. The results indicated that the model under hypoxia conditions reliably reflected the conditions in the invasive form of OSCC and could be used for further research.

Animal models of tumors in vivo, despite their advantages, have certain limitations, such as genetic differences between humans and animals. This is why increasingly complex in vitro models are being created to more accurately reflect clinical conditions. Colley et al. presented the method of creating models of oral dysplasia, cancer in situ, and invasive cancer, using tissue engineering. To generate the models, the researchers used suspensions of CAL-27 and DOK cells as well as FaDu spheroids and then seeded them to full-thickness tissue-engineered oral mucosal models. After 14 days of breeding CAL-27 and DOK, oral dysplasia model was created. However, after an additional 7 days for the CAL-27 line, the cells transcended beyond the basal membrane, creating an invasive OSCC model. The implantation of FaDu spheroids into a healthy oral mucosa gave an image of cancer in situ. Using these models, new methods of treatment, diagnosis, and drug delivery systems could be tested [64].

The breakthrough moment of transition from pre-cancerous lesion to invasive cancer is the cells crossing through the basal membrane. An important factor is modification of the composition of ECM by MMPs. Tristetraprolin (TTP) is a protein affecting the expression level of many pro-inflammatory mediators. Van Tubergen et al. evaluated the effect of TTP loss or inactivation on HNSCC cell (UM-SCC-1) invasion, using an oral-cancer-equivalent (OCE) 3D model and in vivo chorioallantoic membrane (CAM). TTP inactivation occurred as a result of phosphorylation via p38 mitogen-activated protein kinase (p38), which in turn was activated by rap1B. Both TTP phosphorylation and expression suppression by shRNA resulted in increased secretion of MMP2, MMP9, and Il-6 fostering the invasion. Therapy focused on rap1-p38-TTP cascade is promising due to its impact on multiple proinflammatory mediators [65].

A new technique of obtaining and establishing cancer organoid lines is the Cancer Tissue-Originated Spheroids (CTOS) method, successfully used in colon, lung, and bladder cancer [66–68]. The cell lines obtained from patients are cultured as organoids. Tanaka et al. demonstrated the establishment of HNSCC organoids from 43 patient samples. The authors analyzed the organoids using different methods: immunohistochemistry, Western Blotting, drug sensitivity assays, clonogenic survival assays, and animal experiments. They successfully established HNSCC organoids at 30.2% and 2D cell lines at 53.8% success rate. They concluded that organoids could work as a method for the identification of useful biomarkers, predict in vivo drug sensitivity and were a valuable method of improving an individualized HNSCC treatment [69].

Hagemann et al. also analyzed in vitro methods to assess the HNSCC cell line's response to various therapy regimens. The authors revealed that cell viability and spheroid size are indicators of susceptibility to oncological methods and thus could be used to assess patient response to therapy, which serves as a valuable and cost-efficient tool for a personalized treatment of HNSCC [70]. Hagemann concluded that it is necessary to implement multicellular spheroids from different HNSCC cell lines and establish a trustworthy protocol to measure spheroid size and viability because of the effectiveness and complex mechanisms behind various oncological treatments, including drug resistance. Their recommendations were to use spheroid cell culture models in a preclinical setting [71].

Stanton et al. emphasized that HNSCC cell lines established microenvironments resulting in various proliferation rates, metabolic activities, and mitochondrial functional activities between outer layers and cell interiors. The authors revealed that multicellular tumor spheroid (MCTS) cultures represented more physiologically applicable in vitro cell tumor models that imitated both the microenvironments and interactions between cells and cell-ECM relations, which appear in solid tumors, and could be transformed into in vivo animal models and patients [72].

All cells, including cancer cells, release extracellular vesicles (EVs) containing peptides, lipids, or nucleic acids. They serve for intercellular communication, which may affect the immune response. Al Samadi et al. conducted research on two cell lines of tongue cancer: HSC-3 (highly invasive) and SCC-25 (less invasive). The cells were co-cultured with immune cells in a 3D form, using human leiomyoma discs and Myogel. It was shown that activated immune cells caused a reduction of proliferation in both cell lines and reduction of invasiveness of HSC-3. The researchers also studied the impact of EVs derived from cancer cells on the cytotoxicity of CD8 + T and NK cells. Cytotoxicity was increased for EVs from both lines, but for SCC-25, the effect was stronger [73].

The above-mentioned studies on a two-dimensional model confirmed the validity of using nano delivery in cancer therapy. In turn, Besic Gyenge et al. conducted research on cellular uptake, intracellular distribution, and cytotoxicity of modified silica nanoparticles containing tris(bipyridine)ruthenium(II) dichloride in HNSCC (UMB-SCC-745) cells in both 2D and 3D forms. Three modifications of the nanoparticle surface were used for the study: hydroxylated ($Ru@SiO_2$-OH), aminopropylated ($Ru@SiO_2$-NH_2) and PEGylated ($Ru@SiO_2$-PEG). As a preliminary condition for further studies, the concentration that did not cause a statistically significant change in cell proliferation was determined. Using confocal and transmission microscopes, the cellular uptake of $Ru@SiO_2$-OH and $Ru@SiO_2$-NH_2 was observed after 30 min of testing and the particles were in vesicles bound to the cell membrane. The cellular uptake of $Ru@SiO_2$-PEG was minimal and, therefore, excluded from further research. Immunohistochemical studies showed that most of the nanoparticles were in large organelles with low participation of early endosomes. However, in the 3D model study, it turned out that nanoparticles, regardless of surface modification, were located only in the outer layer of the cells, which suggested that they were not actively secreted into the intercellular space. In the case of therapy of solid and poorly vascularized tumors, it is necessary to look for other delivery methods that can be transmitted intercellularly [74].

Another way to deliver chemotherapeutic agents to cancer cells is to encapsulate them in polymersomes, as they are shown to accumulate better in tumor tissue and have a longer half-life than PEGylated

liposomes. Colley et al. investigated the possibility of using poly(2-(methacryloyloxy) ethyl phosphorylcholine) (PMPC) and poly(2-(diisopropylamino) ethyl methacrylate) (PDPA) polymersomes in the delivery of doxorubicin and paclitaxel to HNSCC cells. The tests were conducted both on monolayer cultures and 3D forms of CAL-27 and FaDu cells. The results were compared with those obtained for normal oral keratinocytes, fibroblasts, and human dermal fibroblasts. Faster cellular uptake of the encapsulated drug form occurred in the HNSCC cells due to a higher expression of B scavenger receptors through which polymersomes are internalized. In the study on 2D models, it was shown that short incubation with drug-loaded polymersomes induced strong cytotoxic activity. As far as the research on spheroids is concerned, it was shown that polymersomes with encapsulated drugs penetrated deeply into the 3D culture, causing serious cell damage [75].

In turn, Hinger et al. analyzed the possibility of using a new lipid nanostructured carrier called Lipidot to deliver mTHPC to tumor cells. Tongue cancer cell line CAL-33 was cultured in the form of spheroids, in which the applicability of Lipidotes in PDT was determined. The study used two carrier sizes, namely 50 nm and 120 nm diameter mTHPC-loaded (M-Lipidots) nanoparticles compared to free PS. Using confocal scanning microscopy, slower cellular uptake of the encapsulated PS form was found. For 120 nm Lipidotes, penetration into the spheroids was slower than those of 50 nm. The researchers demonstrated a lack of toxicity of the unloaded carrier and reduced dark cytotoxicity of the encapsulated form compared to free mTHPC. In a phototoxicity study, the cells with mTHPC or M-Lipidots were incubated at 3.67, 7.34 and 14.69 μM for 24 h and then exposed to visible light for 20 min. As it turned out, 50 nm M-lipidots showed efficacy similar to free PS. At higher concentrations, they caused complete disintegration of the spheroids. As far as 120 nm of M-lipidots are concerned, even at the highest concentration, a reduction of the spheroids was observed by only 34%. ATP luciferase viability assay confirmed these results. Cell viability at 14.69 μM was 1.8%, 6.6%, and 66.2% for free mTHPC, 50 nm M-lipidots, and 120 nm M-lipidots respectively. For the free PS, cell death occurred both by necrosis and apoptosis, and for the encapsulated form only by apoptosis [76].

Anti-cancer therapy can lead to nervous tissue damage. Examples of damaging processes are demineralization caused by radiotherapy or mechanical impair during surgery. A major advantage of PDT is the protection of nerve functions. One of the new methods used for the delivery of drugs to cancer cells is photochemical internalization (PCI) that involves a small dose of PDT, which selectively destroys lysosomes and allowing for intracellular drug release. O'Rourke et al. studied the neuronal toxicity of PCI on 3D dorsal root ganglion (DRG) and satellite glia models and then compared it with cytotoxicity towards OSCC on the PCI30 line. Two PSs – *meso*-tetraphenylporphine (TPPS2a) or tetraphenylchlorin disulfonate (TPCS2a), and the glycopeptidic antibiotic Bleomycinwere used for PCI therapy. It was found that neurons survived under conditions sufficient to destroy cancer cells [77].

Quantum dots (QDs) are nanoparticles characterized by their ability to fluoresce with high brightness. The properties of QDs allow for their inclusion in fluorescence guided surgery as well as in PDT. Their wider use is limited by poor biocompatibility and strong hydrophobic properties. Mangeolle et al. conducted research on OSCC (KB) and lung cancer (A549) spheroids, using QDs conjugated with folic acid to improve targeting. Many cancer cells, including the KB line, overexpressed receptor-α folate (FR-α). In turn, A549 line is FR- α negative and was used as a control group. Epifluorescent microscopy analysis revealed strong QD-FA uptake in the KB cells. For comparison, no fluorescence was found for the A549 and KB cells with saturated receptors by preincubation with folic acid. The researchers showed an increase of the QD-FA uptake in the KB spheroids compared to the non-targeted QDs. The QDs were mainly located in the outer layers of the cells and did not exceed 100 nm of depth [78].

An important condition for the creation of effective anti-cancer therapy is the determination of the molecular basis of the disease. A new S100A16 protein expression has been found in cancer cells and its role in cancer progression is being tested. Sapkota et al. conducted clinical trials in which a lower level of expression of this protein was found in OSCC than in the normal oral mucosa with an average level in dysplastic lesions. Two clones of H357 and CaLH3 cells were created, using retroviruses and shRNA. The first one was over-expressed and the second one knocked down. In in vitro experiments on the 3D models of these cells, it was found that the overexpression resulted in a reduction in the ability to create spheres and in an invasive potential. These results correlated with the reduction of the number of markers of self-renewal (Bmi-1 and Oct 4A) and the level of MMP1 mRNA and MMP9 mRNA.

4. Studies on CAM model

Chick Chorioallantoic Membrane (CAM) is a simple model which offers new advantages for the study of blood vessels. During the last decade, it has become a preclinical in vivo model for the drug assessment of vascular growth and their response to a variety of therapeutic methods and substances. The first procedure on the CAM model was presented by Rous and Murphy in 1911 and 1912. They transplanted sarcoma tumors and performed heterologous transplantations of tumors onto the CAM model in chicken embryos. Then, the CAM was explored for viruses and bacteria culture and it rapidly developed as a valuable model system for vascular analysis. The CAM model allows the real-time visualization of different in vivo processes without bioethical committee and/or animal protocol approvals. It is cost-effective, reproducible, reliable, easy to take control of the interference and imaging of the vasculature, using microscopy, computed tomography (CT), magnetic resonance (MRI), positron emission tomography imaging (PET) or the fluorescence imaging (FI) [79–81].

The CAM model enables understanding of reactions of the vascular endothelium. At the same time, it is an inexpensive and accessible model for laboratory implementation. It could serve as an alternative for animal models, especially in that no neural receptors are developed and no pain is being made to the embryo until it reaches two weeks [82].

The CAM model has some advantages over the animal model where cancer cells are directly implanted into connective tissue, bypassing the first barrier of invasion — the basal membrane. In the CAM model, cancer cells are sown on the surface of the embryo. To grow in the connective tissue and metastasis, they must overcome the barrier that the basal membrane creates. Liu et al. used HNSCC cells (UM-SCC-29) for a study in which they evaluated the effect of an expression enhancer of zeste homolog 2 (EZH2) on tumor development in the CAM model. They found that in the case of EZH2-knockdown cells with shRNA, tumor growth was significantly reduced. In addition, the researchers showed a decreased area of the vessels adjacent to the tumor in the case of the EZH2-knockdown cells. The cells with a higher EZH2 expression presented greater invasiveness due to the destruction of the basal membrane and higher ability to metastasis [83].

Tumor development is inextricably linked to angiogenesis and vascular development is necessary for both tumor growth and metastasis. Hence, the dominance of the CAM model over cell cultures, in which the vascular response to the treatment can be studied. Buzza et al. investigated vascular response to PDT, using two PSs: Photogem® from the porphyrin group and Photodithazine® from the group of chlorins, at concentrations of 0.1–100 μg/cm^2. Photogem® and Photodithazine® were irradiated with two diode lasers emitting light at 630 nm and 660 nm wavelengths respectively. Exposure conditions were as follows: light doses in a range of 4.8–40 J/cm^2 and light irradiance from 80 to 100 mW/cm^2. Vascular changes were evaluated after 0–300 minutes of PDT. The results indicated that intravascular administration was more effective than the local application. A faster and more visible PDT effect in the form of vessel closure was observed for chlorin.

In turn, Chin et al. in their research on 2D cell cultures evaluated the effect of synthesized ZnPc derivatives on the vascular effect in the CAM model and compared it with ZnPcS4. The PSs were administered intravenously and then exposed to light at a wavelength of 600–800 nm and a light dose of 5 or 10 J/cm^2. Immediately after the treatment, the vascular effect was assessed based on the ability to close blood vessels depending on their diameter. Only compound 2 and 3 were tested because compound 1 precipitated in the vessels. Phthalocyanine 3 was more effective in vascular occlusion than phthalocyanine 2, while both produced more pronounced vascular effects than ZnPcS4, which correlates with data obtained from in vitro studies. In none of the cases was complete vessel closure found in the CAM model [50].

Kuzyniak et al. also studied the efficacy of ZnPC derivative in PDT. Phthalocyanine was created by substituting tetra-triethyleneoxysulfonyl group. In the first part of their research, they assessed the usefulness of a PS in PDT on gastrointestinal cancer cells, showing strong phototoxic activity and suppression of proliferation by induction of apoptosis. In studies on the CAM model, at day 11 of development, the PS was applied topically at a concentration of 10 μM. Then, after 24 h, 10 J/cm^2 light was applied from a broadband white light source and after the next day, vascular changes were assessed, using intravital microscopy. A reduction of blood perfusion by the degeneration of blood vessels and capillaries was also observed [84].

In their next study, Kuzyniak et al. implanted plaques of esophageal SCC(KYSE-140) cells into the CAM model on day 7 of development. After 72 h, PDT was used under the same conditions as in the previous study. Tumors were excised 72 h after irradiation and then changes in volume were assessed. There was a 70% reduction in tumor volume compared to the control group in which physiological saline was given instead of a PS. Similar antiangiogenic activity was observed as in the previous study [85].

There are many tumor cell lines and tumor tissues (HTC-116, SW480, SW620, Saos-2 and SW1353, M21-L, neuroblastoma) which have been successfully used in the CAM model to study tumor growth. Some new CAM models have been introduced and tested on HNSCC and OSCC [86–88].

Adar et al. performed a study on human ovarian carcinoma (A2780) using spheroid inoculation technique and revealed that with the use of imidazoacridinone (IA) PDT led to selective destruction of tumors and their associated vasculature [86].

Subauste et al. conducted an experiment with colon cancer cell lines, namely SW480 and SW620 which demonstrated that CAM fixed high levels of VEGF-dependent angiogenesis induced by both colon cancer cell lines. The author highlighted that CAM delivered alternate approaches to conventional mammalian model systems for the assessment of new anti-cancer therapeutic options [87].

Gronau et al. studied HNSCC using CAM performing an experiment to assess the efficacy of cisplatin cytotoxicity. Using this method, the author revealed that incubation with cisplatin caused a decrease in viability by 49% after 24 and 48 h [88].

Anti-angiogenesis is a promising alternative in cancer treatment. One potent suppressor of tumor angiogenesis in OSCC is the axonal sprouting inhibitor semaphorin 3A (Sema3A). Chao Huang et al. used tongue squamous cell carcinoma cell line (SSC-9) and performed an angiogenesis assay with endothelial cell tube formation method and CAM analysis. The authors used a tumor xenograft model to evaluate the effect of Sema3A on tumor growth. Using Western Blot, they studied the mechanisms of inhibiting angiogenesis by Sema3A. The researchers revealed that the overexpression of Sema3A in OSCC cells inhibited tumor growth by reducing angiogenesis [89].

As PDT is also used to treat vascular diseases, one of the mechanisms of PDT is the closure of blood vessels. Using CAM models, it is possible to perform an analysis with many PSs to recognize photodynamic vascular effects. Chen et al. performed an experiment to estimate the effect of curcumin applied topically with 0.1–10 mM/cm^2 irradiation in the CAM model. Irradiation was performed at a wavelength of 450 nm, 50 mW/cm^{2}fluence rate and with 30 J/cm^2 fluence for 10 min. The vascular effect was tracked with vessel images quantitatively analyzed with MatLAB, each obtained after 30 min in the first 3, 12, and 24 h. The researchers concluded that curcumin revealed an angio-inhibitory effect, and combined with irradiation (Curcumin-PDT) induced an advanced vascular effect. Curcumin induced the same effect without irradiation [90].

Some authors reported that in the CAM model, the response of PDT is proportional to the delivered dose of light and to the concentration of PS [91,92]. In addition, CAM was also used to examine the association between tissue oxygen concentration during PDT and the subsequent vascular injury [93].

Huntosova et al. used human ovarian carcinoma (A2780) cells to establish tumor xenografts onto CAM. The authors performed measurements of pO_2 and provided evidence that the new PS – Ru(Phen) – had fast pharmacokinetics but very low in vivo phototoxicity. Furthermore, they demonstrated that Ru(Phen) luminescence lifetimes showed linear Stern-Volmer oxygen dependencies in various microenvironments (blood, serum, in vivoin the intra/extravascular space of CAM) [94].

In a study by Lim et al., PDT with a semi-synthesized analogue 15(1)-hydroxypurpurin-7-lactone dimethyl ester termed G2 was used on the CAM model in order to estimate the preclinical potential of G2 as a PS. The authors report that G2 accumulation peaked within the first minute and its extravasation from intra- to extra-vascular arose gentler in comparison to Verteporfin. They observed the shutting off of not only capillaries and small vessels, but also large ones after treatment with 4 μg of G2 with 20 J/cm^2 fluence at 400–440 nm wavelengths and 40 mW cm^2 fluence rate. They concluded that G2 had the potential to be developed as a therapeutic agent for PDT, AMD, and cancer [92].

The aim of the Park et al. study was to examine if PDT using hexenyl ester of 5-aminolaevulinic acid (ALA-hx) had a cytotoxic effect on salivary gland adenocarcinoma SGT cells. They used the MTT test, a gene expression of Coproporphyrinogen oxidase (CPO), ROS production by flow cytometry, and in vivo CAM for assessment. The authors confirmed that ALA-hx PDT suppressed proliferation of SGT cells, induced CPO mRNA expression, and ROS. The tests performed in vivo on CAM also confirmed ALA-hx PDT tumor destruction [95].

Kauffmann et al. performed a study to integrate CAM as a consistent in vivo model for the assessment of 350–450 μm thick slices of OSCC tumor to investigate growth after topical induction, using the proinflammatory cytokines: tumor necrosis factor α (TNFα) and transforming growth factor β (TGFβ). The authors estimated tumor growth and assessed immunohistochemical examinations of E-cadherin and vimentin, which were used as Epithelial-to-mesenchymal transition (EMT)-makers. After TNFα induction, tumors in stage T1 and T2 demonstrated higher E-cadherin expression but also reduction of vimentin; E-cadherin expression decreased and vimentin increased in larger tumors in the T3 and T4 stage. TGFβ induction also led to an increased release of vimentin in T3 and T4 tumors and N1 and N2b stages. The authors concluded that E-cadherin and vimentin were not adequate to represent the complexity of the EMT in this model, and further molecular and signaling trail studies were essential [96].

Low-density lipoproteins (LDL) are major plasma cholesterol transporters. Cholesterol is needed for cells to grow because it is a building block of the cell membrane. Due to increased metabolism and cell growth, cancer cells usually have an increased need for cholesterol. Burikova et al. investigated the pharmacokinetics of hypericin (Hyp) in an environment containing LDL on a CAM model with implanted esophageal SCC(TE-1) spheroids. The spheroids were implanted on day 7 of development of the embryo and after an additional 24 h, free Hyp and LDL-Hy were applied. Both free-Hyp and LDL-Hyp clearly visualized the tumor spheroids. An increase in fluorescence correlated with time in the observation lasting six hours. The study showed an improvement in pharmacokinetics in the presence of LDL. For LDL-Hyp, the contrast between healthy tissue and tumor changes was increased

[97].

5. Summary

Due to the persistence of high incidence and mortality from OSCC as well as limitations imposed by the classical methods, new ways of treatment are being sought. One promising alternative, especially for the initial clinical stages of cancer, is PDT. Before clinical trials, each new method must pass several tests confirming its validity. The first stage of testing is in vitro studies on cancer cell lines which enables the evaluation of the effects of therapy at the cellular and molecular level. In studies on 2D models, most researchers evaluated the viability of cancer cells after exposure to PDT, resulting in a significant reduction of cell survival, despite the use of different protocols. The main cytotoxic effect of PDT is related to the fragmentation of DNA and apoptosis. A promising direction in the development of PDT seems to be the use of nanotechnology which makes it is possible to improve the pharmacokinetics of PSs, increase the selectivity of uptake, or use NIR for irradiation.

Despite the advantages, the 2D model has its limitations such as artificial environment parameters or inability to mimic conditions of physiological cell-cell interactions observed in solid tumors. Spheroids reflect the clinical conditions better due to the presence of ECM and the ability to imitate the microenvironment of a solid tumor. After applying PDT to a spheroidal model, the inhibition of spheroid growth and disintegration are observed.

The described studies on CAM models indicate that it is a useful tool for determining vascular changes after PDT. In addition to direct cytotoxicity against cancer cells, the vascular effect is an important treatment result, which authors most often described as occlusion of blood vessels. The studies on chicken embryos also enable assessment of angiogenesis, invasion, metastasis after the implantation of cancer cells, and changes in volume of tumors inoculated into the CAM after PDT.

The research results on 2D and 3D cell lines as well as with CAM models indicate the efficacy of PDT against OSCC and make it possible to expect positive results in clinical trials. For confirmation, it will be necessary to present the results of studies on animal models and clinical tests.

Conflict of interest

The authors have no conflict of interest to declare.

Acknowledgement

The authors received no financial support for the study and authorship.

References

[1] A.C. Chi, T.A. Day, B.W. Neville, Oral cavity and oropharyngeal squamous cell carcinoma–an update, CA Cancer J. Clin. 65 (5) (2015) 401–421.
[2] Y. Ariyoshi, M. Shimahara, K. Omura, E. Yamamoto, H. Mizuki, H. Chiba, Y. Imai, S. Fujita, M. Shinohara, K. Seto, Japanese Society of Oral and Maxillofacial Surgeons, Epidemiological study of malignant tumors in the oral and maxillofacial region: survey of member institutions of the Japanese Society of Oral and Maxillofacial Surgeons, 2002, Int. J. Clin. Oncol. 13 (3) (2008) 220–228.
[3] S. Warnakulasuriya, Living with oral cancer: epidemiology with particular reference to prevalence and life-style changes that influence survival, Oral Oncol. 46 (6) (2010) 407–410.
[4] J.V. Bagan, C. Scully, Recent advances in Oral Oncology 2007: epidemiology, aetiopathogenesis, diagnosis and prognostication, Oral Oncol. 44 (2) (2008) 103–108.
[5] N. Cohen, S. Fedewa, A.Y. Chen, Epidemiology and demographics of the head and neck cancer population, Oral Maxillofac. Surg. Clin. North Am. 30 (4) (2018) 381–395.
[6] Y.A. Lee, S. Li, Y. Chen, Q. Li, C.J. Chen, W.L. Hsu, P.J. Lou, C. Zhu, J. Pan, H. Shen, H. Ma, L. Cai, B. He, Y. Wang, X. Zhou, Q. Ji, B. Zhou, W. Wu, J. Ma, P. Boffetta, Z.F. Zhang, M. Dai, M. Hashibe, Tobacco smoking, alcohol drinking, betel quid chewing, and the risk of head and neck cancer in an East Asian population, Head Neck 41 (1) (2019) 92–102.
[7] U. Mons, T. Gredner, G. Behrens, C. Stock, H. Brenner, Cancers due to smoking and high alcohol consumption, Dtsch Arztebl Int. 115 (35-36) (2018) 571–577.
[8] K. Omura, Current status of oral cancer treatment strategies: surgical treatments for oral squamous cell carcinoma, Int. J. Clin. Oncol. 19 (3) (2014) 423–430.
[9] R. Philips, D. Martin, A. Eskander, J. Schord, N. Brown, S. Zhao, G. Brock, B. Kumar, R. Carrau, E. Ozer, A. Agrawal, S.Y. Kang, J.W. Rocco, D. Schuller, S. Ali, D. Blakaj, A. Bhatt, J. Grecula, T. Teknos, V. Diavolitsis, M. Old, Effect of adjuvant radiotherapy treatment center volume on overall survival, Oral Oncol. 78 (2018) 46–51.
[10] J. Ha, I.Y. Sung, J.H. Son, M. Stone, R. Ord, Y.C. Cho, Analysis of speech and tongue motion in normal and post-glossectomy speaker using cine MRIA, J. Appl. Oral Sci. 24 (5) (2016) 472–480.
[11] T. Bundgaard, O. Tandrup, O. Elbrønd, A functional evaluation of patients treated for oral cancer. A prospective study, Int. J. Oral Maxillofac. Surg. 22 (1) (1993) 28–34.
[12] A.B. Villaret, J. Cappiello, C. Piazza, B. Pedruzzi, P. Nicolai, Quality of life in patients treated for cancer of the oral cavity requiring reconstruction: a prospective study, Acta Otorhinolaryngol. Ital. 28 (3) (2008) 120–125.
[13] H.J. Nyst, I.B. Tan, F.A. Stewart, A.J. Balm, Is photodynamic therapy a good alternative to surgery and radiotherapy in the treatment of head and neck cancer? Photodiagnosis Photodyn. Ther. 6 (1) (2009) 3–11.
[14] S. Kakoei, A.A. Haghdoost, M. Rad, S. Mohammadalizadeh, N. Pourdamghan, M. Nakhaei, M. Bahador, Xerostomia after radiotherapy and its effect on quality of life in head and neck cancer patients, Arch. Iran. Med. 15 (4) (2012) 214–218.
[15] H.Y. Sroussi, J.B. Epstein, R.J. Bensadoun, D.P. Saunders, R.V. Lalla, C.A. Migliorati, N. Heaivilin, Z.S. Zumsteg, Common oral complications of head and neck cancer radiation therapy: mucositis, infections, saliva change, fibrosis, sensory dysfunctions, dental caries, periodontal disease, and osteoradionecrosis, Cancer Med. 6 (12) (2017) 2918–2931.
[16] S.I. Kvaal, T. Warloe, Photodynamic treatment of oral lesions, J. Environ. Pathol. Toxicol. Oncol. 26 (2) (2007) 127–133.
[17] L. Chau, J.T. Jabara, W. Lai, P.F. Svider, B.M. Warner, H.S. Lin, S.N. Raza, A.M. Fribley, Topical agents for oral cancer chemoprevention: a systematic review of the literature, Oral Oncol. 67 (2017) 153–159.
[18] R.R. Allison, K. Moghissi, Photodynamic therapy (PDT): PDT mechanisms, Clin. Endosc. 46 (1) (2013) 24–29.
[19] S. Kwiatkowski, B. Knap, D. Przystupski, J. Saczko, E. Kędzierska, K. Knap-Czop, J. Kotlińska, O. Michel, K. Kotowski, J. Kulbacka, Photodynamic therapy - mechanisms, photosensitizers and combinations, Biomed. Pharmacother. 106 (2018) 1098–1107.
[20] T.J. Dougherty, C.J. Gomer, B.W. Henderson, G. Jori, D. Kessel, M. Korbelik, J. Moan, Q. Peng, Photodynamic therapy, J. Natl. Cancer Inst. 90 (12) (1998) 889–905.
[21] B. Karakullukcu, S.D. Stoker, A.P. Wildeman, M.P. Copper, M.A. Wildeman, I.B. Tan, A matched cohort comparison of mTHPC-mediated photodynamic therapy and trans-oral surgery of early stage oral cavity squamous cell cancer, Eur. Arch. Otorhinolaryngol. 270 (3) (2013) 1093–1097.
[22] H. Choi, W. Lim, J.E. Kim, I. Kim, J. Jeong, Y. Ko, J. Song, S. You, D. Kim, M. Kim, B.K. Kim, O. Kim, Cell death and intracellular distribution of hematoporphyrin in a KB cell line, Photomed. Laser Surg. 27 (3) (2009) 453–460.
[23] X. Lai, F. Ning, X. Xia, D. Wang, L. Tang, J. Hu, J. Wu, J. Liu, X. Li, HMME combined with green light-emitting diode irradiation results in efficient apoptosis on human tongue squamous cell carcinoma, Lasers Med. Sci. 30 (7) (2015) 1941–1948.
[24] E.E. Kelley, F.E. Domann, G.R. Buettner, L.W. Oberley, C.P. Burns, Increased efficacy of in vitro Photofrin photosensitization of human oral squamous cell carcinoma by iron and ascorbate, J. Photochem. Photobiol. B 40 (3) (1997) 273–277.
[25] C.Y. Fang, P.Y. Chen, D.C. Ho, L.L. Tsai, P.L. Hsieh, M.Y. Lu, C.C. Yu, C.H. Yu, miR-145 mediates the anti-cancer stemness effect of photodynamic therapy with 5-aminolevulinic acid (ALA) in oral cancer cells, J. Formos. Med. Assoc. 117 (8) (2018) 738–742.
[26] S. Sharma, A. Jajoo, A. Dube, 5-Aminolevulinic acid-induced protoporphyrin-IX accumulation and associated phototoxicity in macrophages and oral cancer cell lines, J. Photochem. Photobiol. B 88 (2-3) (2007) 156–162.
[27] J.C. Tsai, C.P. Chiang, H.M. Chen, S.B. Huang, C.W. Wang, M.I. Lee, Y.C. Hsu, C.T. Chen, T. Tsai, Photodynamic therapy of oral dysplasia with topical 5-aminolevulinic acid and light-emitting diode array, Lasers Surg. Med. 34 (1) (2004) 18–24.
[28] T.H. Yang, C.T. Chen, C.P. Wang, P.J. Lou, Photodynamic therapy suppresses the migration and invasion of head and neck cancer cells in vitro, Oral Oncol. 43 (4) (2007) 358–365.
[29] D.F. Yang, J.H. Chen, C.P. Chiang, Z. Huang, J.W. Lee, C.J. Liu, J.L. Chang, Y.C. Hsu, Improve efficacy of topical ALA-PDT by calcipotriol through up-regulation of coproporphyrinogen oxidase, Photodiagnosis Photodyn. Ther. 11 (3) (2014) 331–341.
[30] D.F. Yang, J.W. Lee, H.M. Chen, Z. Huang, Y.C. Hsu, Methotrexate enhances 5-aminolevulinic acid-mediated photodynamic therapy-induced killing of human SCC4 cells by upregulation of coproporphyrinogen oxidase, J. Formos. Med. Assoc. 113 (2) (2014) 88–93.
[31] M. Yamamoto, H. Fujita, N. Katase, K. Inoue, H. Nagatsuka, K. Utsumi, J. Sasaki, H. Ohuchi, Improvement of the efficacy of 5-aminolevulinic acid-mediated photodynamic treatment in human oral squamous cell carcinoma HSC-4, Acta Med. Okayama 67 (3) (2013) 153–164.
[32] H.M. Chen, C.M. Liu, H. Yang, H.Y. Chou, C.P. Chiang, M.Y. Kuo, 5-aminolevulinic acid induce apoptosis via NF-kappaB/JNK pathway in human oral cancer Ca9-22 cells, J. Oral Pathol. Med. 40 (6) (2011) 483–489.
[33] Y.H. Moon, J.H. Park, S.A. Kim, J.B. Lee, S.G. Ahn, J.H. Yoon, Anticancer effect of photodynamic therapy with hexenyl ester of 5-aminolevulinic acid in oral

squamous cell carcinoma, Head Neck 32 (9) (2010) 1136–1142.
[34] Y.Y. Wang, Y.K. Chen, C.S. Hu, L.Y. Xiao, W.L. Huang, T.C. Chi, K.H. Cheng, Y.M. Wang, S.F. Yuan, MAL-PDT inhibits oral precancerous cells and lesions via autophagic cell death, Oral Dis. (2019).
[35] Y. Akita, K. Kozaki, A. Nakagawa, T. Saito, S. Ito, Y. Tamada, S. Fujiwara, N. Nishikawa, K. Uchida, K. Yoshikawa, T. Noguchi, O. Miyaishi, K. Shimozato, S. Saga, Y. Matsumoto, Cyclooxygenase-2 is a possible target of treatment approach in conjunction with photodynamic therapy for various disorders in skin and oral cavity, Br. J. Dermatol. 151 (2) (2004) 472–480.
[36] H. Nakagawa, T. Matsumiya, H. Sakaki, T. Imaizumi, K. Kubota, A. Kusumi, W. Kobayashi, H. Kimura, Expression of vascular endothelial growth factor by photodynamic therapy with mono-L-aspartyl chlorin e6 (NPe6) in oral squamous cell carcinoma, Oral Oncol. 43 (6) (2007) 544–550.
[37] A. Sharwani, W. Jerjes, C. Hopper, M.P. Lewis, M. El-Maaytah, H.S. Khalil, A.J. Macrobert, T. Upile, V. Salih, Photodynamic therapy down-regulates the invasion promoting factors in human oral cancer, Arch. Oral Biol. 51 (12) (2006) 1104–1111.
[38] R. Bhuvaneswari, Q.F. Ng, P.S. Thong, K.C. Soo, Nimotuzumab increases the antitumor effect of photodynamic therapy in an oral tumor model, Oncotarget 6 (15) (2015) 13487–13505.
[39] P. Li, G. Zhou, X. Zhu, G. Li, P. Yan, L. Shen, Q. Xu, M.R. Hamblin, Photodynamic therapy with hyperbranched poly(ether-ester) chlorin(e6) nanoparticles on human tongue carcinoma CAL-27 cells, Photodiagn. Photodyn. Ther. 9 (1) (2012) 76–82.
[40] M. Date, I. Sakata, K. Fukuchi, K. Ohura, Y. Azuma, M. Shinohara, K. Matsuzaki, Y. Namiki, H. Takahashi, Photodynamic therapy for human oral squamous cell carcinoma and xenografts using a new photosensitizer, PAD-S31, Lasers Surg. Med. 33 (1) (2003) 57–63.
[41] M.Y. Ahn, H.E. Yoon, S.M. Kwon, J. Lee, S.K. Min, Y.C. Kim, S.G. Ahn, J.H. Yoon, Synthesized Pheophorbide a-mediated photodynamic therapy induced apoptosis and autophagy in human oral squamous carcinoma cells, J. Oral Pathol. Med. 42 (1) (2013) 17–25.
[42] S.A. Kim, M.R. Lee, J.H. Yoon, S.G. Ahn, HOXC6 regulates the antitumor effects of pheophorbide a-based photodynamic therapy in multidrug-resistant oral cancer cells, Int. J. Oncol. 49 (6) (2016) 2421–2430.
[43] S. Moon, J.Y. Bae, H.K. Son, D.Y. Lee, G. Park, H. You, H. Ko, Y.C. Kim, J. Kim, RUNX3 confers sensitivity to pheophorbide a-photodynamic therapy in human oral squamous cell carcinoma cell lines, Lasers Med. Sci. 30 (2) (2015) 499–507.
[44] S.H. Lim, H.B. Lee, A.S. Ho, A new naturally derived photosensitizer and its phototoxicity on head and neck cancer cells, Photochem. Photobiol. 87 (5) (2011) 1152–1158.
[45] H. You, H.E. Yoon, P.H. Jeong, H. Ko, J.H. Yoon, Y.C. Kim, Pheophorbide-a conjugates with cancer-targeting moieties for targeted photodynamic cancer therapy, Bioorg. Med. Chem. 23 (7) (2015) 1453–1462.
[46] L. Song, C. Li, Y. Zou, F. Dai, X. Luo, B. Wang, J. Ni, Q. Liu, O2 and Ca(2+) fluxes as indicators of apoptosis induced by rose bengal-mediated photodynamic therapy in human oral squamous carcinoma cells, Photomed. Laser Surg. 33 (5) (2015) 258–265.
[47] H.J. Lim, C.H. Oh, Indocyanine green-based photodynamic therapy with 785nm light emitting diode for oral squamous cancer cells, Photodiagn. Photodyn. Ther. 8 (4) (2011) 337–342.
[48] A.D. Garg, M. Bose, M.I. Ahmed, W.A. Bonass, S.R. Wood, In vitro studies on erythrosine-based photodynamic therapy of malignant and pre-malignant oral epithelial cells, PLoS One 7 (4) (2012) e34475.
[49] E.C. Tapajos, J.P. Longo, A.R. Simioni, Z.G. Lacava, M.F. Santos, P.C. Morais, A.C. Tedesco, R.B. Azevedo, In vitro photodynamic therapy on human oral keratinocytes using chloroaluminum-phthalocyanine, Oral Oncol. 44 (11) (2008) 1073–1079.
[50] Y. Chin, S.H. Lim, Y. Zorlu, V. Ahsen, L.V. Kiew, L.Y. Chung, F. Dumoulin, H.B. Lee, Improved photodynamic efficacy of Zn(II) phthalocyanines via glycerol substitution, PLoS One 9 (5) (2014) e97894.
[51] K. Beyer, F. Nikfarjam, M. Butting, M. Meissner, A. Konig, A. Ramirez Bosca, R. Kaufmann, D. Heidemann, A. Bernd, S. Kippenberger, N. Zoller, Photodynamic treatment of oral squamous cell carcinoma cells with low curcumin concentrations, J. Cancer 8 (7) (2017) 1271–1283.
[52] Y.Q. Liu, P.S. Meng, H.C. Zhang, X. Liu, M.X. Wang, W.W. Cao, Z. Hu, Z.G. Zhang, Inhibitory effect of aloe emodin mediated photodynamic therapy on human oral mucosa carcinoma in vitro and in vivo, Biomed. Pharmacother. 97 (2018) 697–707.
[53] C.W. Chen, Y.C. Chan, M. Hsiao, R.S. Liu, Plasmon-enhanced photodynamic Cancer therapy by upconversion nanoparticles conjugated with Au nanorods, ACS Appl. Mater. Interfaces 8 (47) (2016) 32108–32119.
[54] S.S. Lucky, N. Muhammad Idris, Z. Li, K. Huang, K.C. Soo, Y. Zhang, Titania coated upconversion nanoparticles for near-infrared light triggered photodynamic therapy, ACS Nano 9 (1) (2015) 191–205.
[55] J. Piskorz, K. Konopka, N. Duzgunes, Z. Gdaniec, J. Mielcarek, T. Goslinski, Diazepinoporphyrazines containing peripheral styryl substituents and their promising nanomolar photodynamic activity against oral cancer cells in liposomal formulations, ChemMedChem 9 (8) (2014) 1775–1782.
[56] M. Wierzchowski, L. Sobotta, P. Skupin-Mrugalska, J. Kruk, W. Jusiak, M. Yee, K. Konopka, N. Duzgunes, E. Tykarska, M. Gdaniec, J. Mielcarek, T. Goslinski, Phthalocyanines functionalized with 2-methyl-5-nitro-1H-imidazolylethoxy and 1,4,7-trioxanonyl moieties and the effect of metronidazole substitution on photocytotoxicity, J. Inorg. Biochem. 127 (2013) 62–72.
[57] A.J. Trinidad, S.J. Hong, Q. Peng, S.J. Madsen, H. Hirschberg, Combined concurrent photodynamic and gold nanoshell loaded macrophage-mediated photothermal therapies: an in vitro study on squamous cell head and neck carcinoma, Lasers Surg. Med. 46 (4) (2014) 310–318.
[58] P. van Driel, M.C. Boonstra, M.D. Slooter, R. Heukers, M.A. Stammes, T.J.A. Snoeks, H.S. de Bruijn, P.J. van Diest, A.L. Vahrmeijer, P.M.P. van Bergen En Henegouwen, C.J.H. van de Velde, C. Lowik, D.J. Robinson, S. Oliveira, EGFR targeted nanobody-photosensitizer conjugates for photodynamic therapy in a pre-clinical model of head and neck cancer, J. Control. Release 229 (2016) 93–105.
[59] M. Hidalgo, F. Amant, A.V. Biankin, E. Budinska, A.T. Byrne, C. Caldas, R.B. Clarke, S. de Jong, J. Jonkers, G.M. Maelandsmo, S. Roman-Roman, J. Seoane, L. Trusolino, A. Villanueva, Patient-derived xenograft models: an emerging platform for translational cancer research, Cancer Discov. 4 (9) (2014) 998–1013.
[60] S. Nurmenniemi, T. Sinikumpu, I. Alahuhta, S. Salo, M. Sutinen, M. Santala, J. Risteli, P. Nyberg, T. Salo, A novel organotypic model mimics the tumor microenvironment, Am. J. Pathol. 175 (3) (2009) 1281–1291.
[61] L. Kadletz, G. Heiduschka, J. Domayer, R. Schmid, E. Enzenhofer, D. Thurnher, Evaluation of spheroid head and neck squamous cell carcinoma cell models in comparison to monolayer cultures, Oncol. Lett. 10 (3) (2015) 1281–1286.
[62] N. Essid, J.C. Chambard, A.B. Elgaaied, Induction of epithelial-mesenchymal transition (EMT) and Gli1 expression in head and neck squamous cell carcinoma (HNSCC) spheroid cultures, Bosn. J. Basic Med. Sci. 18 (4) (2018) 336–346.
[63] Y.S. Hwang, S.Y. Ahn, S. Moon, Z. Zheng, I.H. Cha, J. Kim, X. Zhang, Insulin-like growth factor-II mRNA binding protein-3 and podoplanin expression are associated with bone invasion and prognosis in oral squamous cell carcinoma, Arch. Oral Biol. 69 (2016) 25–32.
[64] H.E. Colley, V. Hearnden, A.V. Jones, P.H. Weinreb, S.M. Violette, S. Macneil, M.H. Thornhill, C. Murdoch, Development of tissue-engineered models of oral dysplasia and early invasive oral squamous cell carcinoma, Br. J. Cancer 105 (10) (2011) 1582–1592.
[65] E.A. Van Tubergen, R. Banerjee, M. Liu, R. Vander Broek, E. Light, S. Kuo, S.E. Feinberg, A.L. Willis, G. Wolf, T. Carey, C. Bradford, M. Prince, F.P. Worden, K.L. Kirkwood, N.J. D'Silva, Inactivation or loss of TTP promotes invasion in head and neck cancer via transcript stabilization and secretion of MMP9, MMP2, and IL-6, Clin. Cancer Res. 19 (5) (2013) 1169–1179.
[66] J. Kondo, H. Endo, H. Okuyama, O. Ishikawa, H. Iishi, M. Tsujii, M. Ohue, M. Inoue, Retaining cell-cell contact enables preparation and culture of spheroids composed of pure primary cancer cells from colorectal cancer, Proc. Natl. Acad. Sci. U. S. A. 108 (15) (2011) 6235–6240.
[67] H. Endo, J. Okami, H. Okuyama, T. Kumagai, J. Uchida, J. Kondo, T. Takehara, Y. Nishizawa, F. Imamura, M. Higashiyama, M. Inoue, Spheroid culture of primary lung cancer cells with neuregulin 1/HER3 pathway activation, J. Thorac. Oncol. 8 (2) (2013) 131–139.
[68] T. Yoshida, H. Okuyama, M. Nakayama, H. Endo, N. Nonomura, K. Nishimura, M. Inoue, High-dose chemotherapeutics of intravesical chemotherapy rapidly induce mitochondrial dysfunction in bladder cancer-derived spheroids, Cancer Sci. 106 (1) (2015) 69–77.
[69] N. Tanaka, A.A. Osman, Y. Takahashi, A. Lindemann, A.A. Patel, M. Zhao, H. Takahashi, J.N. Myers, Head and neck cancer organoids established by modification of the CTOS method can be used to predict in vivo drug sensitivity, Oral Oncol. 87 (2018) 49–57.
[70] J. Hagemann, C. Jacobi, S. Gstoettner, C. Welz, S. Schwenk-Zieger, R. Stauber, S. Strieth, J. Kuenzel, P. Baumeister, S. Becker, Therapy testing in a spheroid-based 3D cell culture model for head and neck squamous cell carcinoma, J. Vis. Exp. 134 (2018).
[71] J. Hagemann, C. Jacobi, M. Hahn, V. Schmid, C. Welz, S. Schwenk-Zieger, R. Stauber, P. Baumeister, S. Becker, Spheroid-based 3D cell cultures enable personalized therapy testing and drug discovery in head and neck cancer, Anticancer Res. 37 (5) (2017) 2201–2210.
[72] S.J. Kochanek, D.A. Close, P.A. Johnston, High content screening characterization of head and neck squamous cell carcinoma multicellular tumor spheroid cultures generated in 384-well ultra-low attachment plates to screen for better cancer drug leads, Assay Drug Dev. Technol. 17 (1) (2019) 17–36.
[73] A. Al-Samadi, S.A. Awad, K. Tuomainen, Y. Zhao, A. Salem, M. Parikka, T. Salo, Crosstalk between tongue carcinoma cells, extracellular vesicles, and immune cells in in vitro and in vivo models, Oncotarget 8 (36) (2017) 60123–60134.
[74] E. Besic Gyenge, X. Darphin, A. Wirth, U. Pieles, H. Walt, M. Bredell, C. Maake, Uptake and fate of surface modified silica nanoparticles in head and neck squamous cell carcinoma, J. Nanobiotechnol. 9 (2011) 32.
[75] P.H. Ahn, J.C. Finlay, S.M. Gallagher-Colombo, H. Quon, B.W. O'Malley Jr., G.S. Weinstein, A. Chalian, K. Malloy, T. Sollecito, M. Greenberg, C.B. Simone 2nd, S. McNulty, A. Lin, T.C. Zhu, V. Livolsi, M. Feldman, R. Mick, K.A. Cengel, T.M. Busch, Lesion oxygenation associates with clinical outcomes in premalignant and early stage head and neck tumors treated on a phase 1 trial of photodynamic therapy, Photodiagn. Photodyn. Ther. 21 (2018) 28–35.
[76] D. Hinger, F. Navarro, A. Kach, J.S. Thomann, F. Mittler, A.C. Couffin, C. Maake, Photoinduced effects of m-tetrahydroxyphenylchlorin loaded lipid nanoemulsions on multicellular tumor spheroids, J. Nanobiotechnol. 14 (1) (2016) 68.
[77] C. O'Rourke, C. Hopper, A.J. MacRobert, J.B. Phillips, J.H. Woodhams, Could clinical photochemical internalisation be optimised to avoid neuronal toxicity? Int. J. Pharm. 528 (1-2) (2017) 133–143.
[78] T. Mangeolle, I. Yakavets, N. Lequeux, T. Pons, L. Bezdetnaya, F. Marchal, the targeting ability of fluorescent quantum dots to the folate receptor rich tumors, Photodiagn. Photodyn. Ther. (2019).
[79] D. Ribatti, The chick embryo chorioallantoic membrane in the study of tumor angiogenesis, Rom. J. Morphol. Embryol. 49 (2) (2008) 131–135.
[80] D.S. Dohle, S.D. Pasa, S. Gustmann, M. Laub, J.H. Wissler, H.P. Jennissen, N. Dunker, Chick ex ovo culture and ex ovo CAM assay: how it really works, J. Vis. Exp. 33 (2009).
[81] P. Nowak-Sliwinska, T. Segura, M.L. Iruela-Arispe, The chicken chorioallantoic

membrane model in biology, medicine and bioengineering, Angiogenesis 17 (4) (2014) 779–804.
[82] T.A. Jones, S.M. Jones, K.C. Paggett, Emergence of hearing in the chicken embryo, J. Neurophysiol. 96 (1) (2006) 128–141.
[83] M. Liu, C.S. Scanlon, R. Banerjee, N. Russo, R.C. Inglehart, A.L. Willis, S.J. Weiss, N.J. D'Silva, The histone methyltransferase EZH2 mediates tumor progression on the chick chorioallantoic membrane assay, a novel model of head and neck squamous cell carcinoma, Transl. Oncol. 6 (3) (2013) 273–281.
[84] W. Kuzyniak, E.A. Ermilov, D. Atilla, A.G. Gurek, B. Nitzsche, K. Derkow, B. Hoffmann, G. Steinemann, V. Ahsen, M. Hopfner, Tetra-triethyleneoxysulfonyl substituted zinc phthalocyanine for photodynamic cancer therapy, Photodiagn. Photodyn. Ther. 13 (2016) 148–157.
[85] W. Kuzyniak, J. Schmidt, W. Glac, J. Berkholz, G. Steinemann, B. Hoffmann, E.A. Ermilov, A.G. Gurek, V. Ahsen, B. Nitzsche, M. Hopfner, Novel zinc phthalocyanine as a promising photosensitizer for photodynamic treatment of esophageal cancer, Int. J. Oncol. 50 (3) (2017) 953–963.
[86] Y. Adar, M. Stark, E.E. Bram, P. Nowak-Sliwinska, H. van den Bergh, G. Szewczyk, T. Sarna, A. Skladanowski, A.W. Griffioen, Y.G. Assaraf, Imidazoacridinone-dependent lysosomal photodestruction: a pharmacological Trojan horse approach to eradicate multidrug-resistant cancers, Cell Death Dis. 3 (2012) e293.
[87] M.C. Subauste, T.A. Kupriyanova, E.M. Conn, V.C. Ardi, J.P. Quigley, E.I. Deryugina, Evaluation of metastatic and angiogenic potentials of human colon carcinoma cells in chick embryo model systems, Clin. Exp. Metastasis 26 (8) (2009) 1033–1047.
[88] S. Gronau, B. Thess, H. Riechelmann, Y. Fischer, A. Schmitt, M. Schmitt, An autologous system for culturing head and neck squamous cell carcinomas for the assessment of cellular therapies on the chorioallantois membrane, Eur. Arch. Otorhinolaryngol. 263 (4) (2006) 308–312.
[89] C. Huang, Y. Wang, J.H. Huang, W. Liu, Sema3A drastically suppresses tumor growth in oral cancer Xenograft model of mice, BMC Pharmacol. Toxicol. 18 (1) (2017) 55.
[90] B. Chen, B.W. Pogue, P.J. Hoopes, T. Hasan, Vascular and cellular targeting for photodynamic therapy, Crit. Rev. Eukaryot. Gene Expr. 16 (4) (2006) 279–305.
[91] E. Debefve, B. Pegaz, H. van den Bergh, G. Wagnieres, N. Lange, J.P. Ballini, Video monitoring of neovessel occlusion induced by photodynamic therapy with verteporfin (Visudyne), in the CAM model, Angiogenesis 11 (3) (2008) 235–243.
[92] S.H. Lim, P. Nowak-Sliwinska, F.A. Kamarulzaman, H. van den Bergh, G. Wagnieres, H.B. Lee, The neovessel occlusion efficacy of 15-hydroxypurpurin-7-lactone dimethyl ester induced with photodynamic therapy, Photochem. Photobiol. 86 (2) (2010) 397–402.
[93] R.S. Seymour, K. Wagner-Amos, Non-invasive measurement of oxygen partial pressure, lateral diffusion and chorioallantoic blood flow under the avian eggshell, Comp. Biochem. Physiol. A Mol. Integr. Physiol. 150 (2) (2008) 258–264.
[94] V. Huntosova, S. Gay, P. Nowak-Sliwinska, S.K. Rajendran, M. Zellweger, H. van den Bergh, G. Wagnieres, In vivo measurement of tissue oxygenation by time-resolved luminescence spectroscopy: advantageous properties of dichlorotris(1, 10-phenanthroline)-ruthenium(II) hydrate, J. Biomed. Opt. 19 (7) (2014) 77004.
[95] J.H. Park, Y.H. Moon, D.J. Kim, S.A. Kim, J.B. Lee, S.G. Ahn, J.H. Yoon, Photodynamic therapy with hexenyl ester of 5-aminolevulinic acid induces necrotic cell death in salivary gland adenocarcinoma cells, Oncol. Rep. 24 (1) (2010) 177–181.
[96] P. Kauffmann, M. Troeltzsch, P. Brockmeyer, H. Bohnenberger, P.I. Heidekruger, M. Manzke, M. Canis, S. Gaayathiri, H. Schliephake, L. Prantl, T. Aung, First experience of chick chorioallantoic membrane (CAM) assay in the clinical work flow with oral squamous cell carcinoma patients, Clin. Hemorheol. Microcirc. 70 (4) (2018) 487–494.
[97] M. Burikova, B. Bilcik, M. Macajova, P. Vyboh, J. Bizik, A. Mateasik, P. Miskovsky, I. Cavarga, Hypericin fluorescence kinetics in the presence of low density lipoproteins: study on quail CAM assay for topical delivery, Gen. Physiol. Biophys. 35 (4) (2016) 459–468.